

Multi-year, spatially extensive, watershed scale synoptic stream chemistry and water quality conditions for six permafrost-underlain Arctic watersheds

5 Arial J. Shogren¹, Jay P. Zarnetske¹, Benjamin W. Abbott², Samuel Bratsman², Brian Brown², Michael P. Carey³, Randy Fulweber⁴, Heather E. Greaves⁴, Emma Haines¹, Frances Iannucci^{4, 5}, Joshua C. Koch³, Alexander Medvedeff⁵, Jonathan A. O'Donnell⁶, Leika Patch², Brett A. Poulin^{7,8}, Tanner J. Williamson¹, William B. Bowden⁵

¹ Earth & Environmental Sciences Department, Michigan State University, East Lansing Michigan 48824, USA

² Plant & Wildlife Sciences Department, Brigham Young University, Provo, Utah, 84602, USA

10 ³ Alaska Science Center, U.S. Geological Survey, Anchorage, Alaska, 99508, USA

⁴ Institute of Arctic Biology, University of Alaska Fairbanks, Fairbanks, Alaska, 99775, USA

⁵ Rubenstein School of Environment and Natural Resources, University of Vermont, Burlington, Vermont 05405, USA

⁶ Arctic Network, National Park Service, Anchorage, Alaska, 99501, USA

⁷ Water Mission Area, U.S. Geological Survey, Boulder, Colorado, 80303, USA

15 ⁸ Department of Environmental Toxicology, University of California Davis, Davis, California, 95616, USA

Correspondence to: Arial J. Shogren (shogrena@msu.edu)

Abstract. Repeated sampling of spatially distributed river chemistry can be used to assess the location, scale, and persistence of carbon and nutrient contributions to watershed exports. Here, we provide a comprehensive set of water chemistry measurements and ecohydrological metrics describing the biogeochemical conditions of permafrost-affected Arctic watersheds. These data were collected in watershed-wide synoptic campaigns in six stream networks across northern Alaska. Three watersheds are associated with the Arctic Long-Term Ecological Research site at Toolik Field Station (TFS), which were sampled seasonally each June and August from 2016 to 2018. Three watersheds were associated with the National Park Service (NPS) of Alaska and the US. Geological Survey (USGS) and were sampled annually from 2015 to 2019. Extensive water chemistry characterization included carbon species, dissolved nutrients, and major ions. The objective of the sampling designs and data acquisition was to characterize terrestrial-aquatic linkages and processing of material in stream networks. The data allow estimation of novel ecohydrological metrics that describe the dominant location, scale, and overall persistence of ecosystem processes in continuous permafrost. These metrics are: (1) subcatchment leverage, (2) variance collapse, and (3) spatial persistence. Raw data are available at the National Parks Service Integrated Resource Management Application portal (<https://doi.org/10.5066/P9SBK2DZ>) and within the Environmental Data Initiative (<https://doi.org/10.6073/pasta/258a44fb9055163dd4dd4371b9dce945>).

35

Plaintext Summary. Rapidly sampling multiple points in an entire river network provides a high-resolution snapshot in time that can reveal where nutrients and carbon are being taken up and released.

Here, we describe two such datasets of river network chemistry in six Arctic watersheds in northern
40 Alaska. We describe how these repeated snapshots can be used as an indicator of ecosystem response to
climate change and to improve predictions of future release of carbon, nutrient, and other solutes.

1 Introduction

Watershed chemistry studies—like all ecosystem studies—involve trade-offs between sampling
extent (i.e., how much area is observed) and spatiotemporal grain (i.e., the resolution of observations in
45 space and time) (Abbott et al., 2018; Burns et al., 2019; Ward et al., 2019). Initial assessments are
typically performed at the plot (terrestrial studies, <1–100 m²) (Keller et al., 2007; Prager et al., 2017)
or reach-scales (stream studies, 100–1000 m), where replicated observations and manipulations can be
made (Kling et al., 2000; Docherty et al., 2018). Trade-offs between extent and grain are especially
apparent in remote settings such as the Arctic, where logistical constraints and high operational costs
50 often force researchers to choose among these sampling approaches (Abbott et al., 2021b). While these
intensive studies are crucial to identifying the underlying processes controlling solute transport and
transformations, it is challenging to scale up plot-level observations to the watershed, regional, or
continental levels (Wiens, 1989; Thrush et al., 1997; Helton et al., 2012). Likewise, large-scale
observations sensed remotely from aircraft or satellites often cannot identify the processes behind the
55 regional to continental patterns they reveal (Newman et al., 2019; Shiklomanov et al., 2019). Bridging
small- and large-scale observations is complicated by both spatial heterogeneity and temporal variation,
as mosaics of diverse ecosystem patches evolve in space and time (Bernhardt et al., 2017; Pinay et al.,
2015; Abbott et al., 2016). Consequently, mechanisms that are observed at the plot- or regional levels
may not reconcile (Kareiva and Andersen, 1988) because connectivity among patches can create
60 emergent patterns and processes (Sivapalan, 2003; McDonnell et al., 2007; Covino, 2017). To

understand and predict ecosystem behavior in the Anthropocene, we need to observe how biogeochemical patterns are produced and propagate across scales. Here, we describe a medium scale watershed chemistry dataset that includes spatially distributed hydrological, ecological, and geochemical properties. Using a synoptic experimental design, we measured these parameters across 65 medium-scale watersheds (<1 to >1000 km²) multiple times over several years. We hope this dataset will help bridge the gap between plot-level and regional investigation of ecosystem change in the permafrost zone.

Most water chemistry and flow assessments conducted in the Arctic and elsewhere are based on observations at river outlets (McClelland et al., 2006, 2007; Tank et al., 2016; Toohey et al., 2016; 70 Shogren et al., 2020; Zarnetske et al., 2018). The flow of water integrates biogeochemical signals, such that river chemistry at the watershed outlet contains information about both terrestrial and aquatic biogeochemical processes that occurred upstream in the network (Temnerud et al., 2010; Vonk et al., 2019; Tank et al., 2020). Indeed, using sampling and monitoring approaches that capture the watershed outlet response over time has logistic and safety advantages for site access. Further, the recent 75 application of novel sensor technology has enabled high-frequency watershed-scale studies (Shogren et al., 2021; Ruhala and Zarnetske, 2017; Khamis et al., 2021). For example, the paired high-frequency flow and a limited set of chemical properties for the watersheds in this data paper are available at the Arctic Data Center (Zarnetske et al., 2020b, c, a). While these watershed outlet measurements can provide insight into possible upstream and upslope processes (Laudon et al., 2017; Shogren et al., 2021; 80 Moatar et al., 2017), they often do not diagnose primary drivers of lateral transport of materials (Burns et al., 2019; Appling et al., 2018; Temnerud et al., 2010; Hoffman et al., 2013; Collier et al., 2018).

These large-scale measurements are the result of variable inputs which are buffered and blurred as multiple spatiotemporal signals are mixed and propagated through the surface and subsurface network (Creed et al., 2015; Abbott et al., 2018; Kolbe et al., 2019). To identify the processes behind those
85 signals, we need to venture into the headwaters, extending our observations into smaller subcatchments that match the spatial scale of mechanisms controlling carbon and nutrient uptake and release (Shogren et al., 2019; Gu et al., 2021; Abbott et al., 2017).

Spatially extensive or “synoptic” sampling frameworks, such as contained in this data paper, provide multiscale information about the source of signals across the entire watershed network, creating
90 a direct complement watershed outlet monitoring. With a synoptic sampling design, researchers can capture the spatial extent of nested subcatchments and therefore assess terrestrial-aquatic transfer of material and stream network processing (Abbott et al., 2018; Shogren et al., 2019; Gu et al., 2021). Though synoptic campaigns are logistically challenging (Yi et al., 2010; Abbott et al., 2021b; Rodríguez-Cardona et al., 2020), the high-resolution spatial snapshot they generate allows empirical
95 assessment of biogeochemical signals at intermediate spatial scales (Abbott et al., 2018; Shogren et al., 2019; McGuire et al., 2014). In recent years, synoptic campaigns have focused on solute distribution in temperate river systems (Gardner and McGlynn, 2009; McGuire et al., 2014; Byrne et al., 2017; Abbott et al., 2018; Dupas et al., 2019). While there have been fewer synoptic campaigns in permafrost systems (Kling et al., 2000; Bowden, 2013; Shogren et al., 2020; Abbott et al., 2015, 2021b; Lamhonwah et al.,
100 2017), their application presents an opportunity to characterize the fate of carbon and nutrients in a rapidly changing Arctic, creating multi-scale targets for the Earth system models used for predicting environmental change (Collier et al., 2018; Koven et al., 2015; Turetsky et al., 2020; Vonk et al., 2015).

Because permafrost degradation is triggering both large-scale deepening of the active layer and discrete permafrost collapse (thermokarst) features (Gao et al., 2021; Turetsky et al., 2020; Farquharson et al., 105 2019), synoptic snapshots could be invaluable in detecting the degree, location, and type of climate response. Therefore, measuring the spatial distribution of water chemistry in high latitude river networks could advance understanding of permafrost ecosystems and improve estimates of ecosystem feedbacks to climate change (Bring et al., 2016; Wrona et al., 2016; Schuur et al., 2015; Mu et al., 2020).

110 The datasets presented here were derived from repeated synoptic samplings in six Arctic watersheds in northern Alaska occurring on three distinct high latitude ecosystem types: Arctic tundra, Boreal forest, and Alpine tundra (Figure 1). In this paper, we illustrate the utility of such data via a set of initial watershed chemistry analyses for ecologically significant reactive solutes including dissolved organic carbon (DOC), nitrogen (e.g., nitrate, N-NO₃⁻; ammonium, N-NH₄⁺; dissolved organic nitrogen, 115 DON; total dissolved nitrogen, TDN), phosphorous (soluble reactive phosphorus, SRP; total dissolved phosphorus, TDP), as well as a suite of geochemically significant anions and cations (e.g., calcium, Ca²⁺; total iron, Fe; dissolved silica, DSi; *see Table 1 for full list of analytes*). In addition, we use these datasets to introduce simple metrics for biogeochemical solutes: *variance collapse*, *subcatchment leverage*, and *spatial persistence* (Abbott et al., 2018; Shogren et al., 2019; Gu et al., 2021; Dupas et al., 120 2019; Frei et al., 2020). These new metrics seek to extract information more fully from rich spatiotemporal water chemistry datasets. Specifically, these metrics characterize what spatial scale is the most relevant in explaining terrestrial-aquatic material flux, how much influence or *leverage* each sampling site has on the watershed budget, and whether individual samplings are adequate to capture

temporal variation. In this light, synoptic sampling frameworks provide robust information about how to
125 scale plot- and reach-level observations while also providing a multi-scale target for remotely sensed
data and numerical models. Ultimately, the information gleaned from these metrics is desired by a range
of disciplines from ecologists to natural resource managers.

First, we use subcatchment leverage to identify nested areas within the network that exert a
disproportionate influence on flux at the watershed outflow (Abbott et al., 2018; Shogren et al., 2019).
130 Subcatchment leverage can be interpreted as the contribution of the subcatchment to watershed mass
flux where the value can be negative (indicating the subcatchment has lower areal flux than the outlet,
decreasing watershed flux), positive (indicating the subcatchment has higher areal flux than the outlet, a
net increase in flux), or zero (no influence because it is the same as the outlet). Estimating leverage
allows identification of specific subcatchments with disproportionate influence on material export,
135 defined here as high leverage. Subcatchments with high leverage behave as a strong source or sink
within the watershed network, strongly influencing the resulting concentrations at the outflow, and can
be selected as sites for further mechanistic study or monitoring. Likewise, the direction and magnitude
of leverage averaged across the entire watershed contains information about net solute removal and
production in the stream network (Shogren et al., 2019). For example, if the mean leverage for the
140 watershed is above zero, this indicates there are more solute sources than can be accounted for at the
watershed outlet, implying there has been solute removal during transport through the network. Second,
we examine what spatial extent or patch size controls solute production and removal by identifying
thresholds of concentration variance collapse (Abbott et al., 2018). We generally expect the amplitude
of solute variability to decrease moving downstream from headwaters to larger systems (Creed et al.,

145 2015) with greater variability among headwaters, whereas downstream reaches are less likely to have
extremely high or low concentrations because they integrate multiple upstream source or sink processes
(Wolock et al., 1997; Temnerud and Bishop, 2005; Burt and Pinay, 2005; Abbott et al., 2017).
Therefore, the size of nutrient sources and sinks in the landscape can be assessed by the spatial scale of
the variance collapse of concentration among watershed reaches (Abbott et al., 2018; Shogren et al.,
150 2019). The threshold of variance collapse is similar to the elementary representative area concept
(Zimmer et al., 2013, p.20), where the threshold represents the spatial scale at which landscape
“patches” or processes throughout the watershed network that produce and remove solutes are
effectively integrated. Lastly, the spatial persistence metric can be used to assess whether a given site is
representative (i.e., the same pattern continues through time), or if patches restructure in space between
155 sampling campaigns (i.e., reorganization of patches requires greater frequency in sampling) (Abbott et
al., 2018; Dupas et al., 2019; Gu et al., 2021). Spatial persistence effectively quantifies the temporal
representativeness of an instantaneous measurement at a given site, potentially indicating the type of
process creating the patterns and informing future watershed study design and data analysis of extant
data (Kling et al., 2000; Shogren et al., 2019).

160 **2 Study Location & Design**

2.1 Study Watersheds

2.1.1 Arctic LTER sites at Toolik Field Station

The Arctic Long-Term Ecological Research site based out of Toolik Field Station (TFS) is in the
foothills of the Brooks Range on the North Slope of Alaska, USA (mean elevation 720 m). We
165 conducted surveys in three watersheds near TFS: the Kuparuk River, Oksrukuyik Creek, and Trevor
Creek. The three study watersheds were chosen because they spanned dominant circumarctic vegetation

types, permafrost characteristics, and hydrologic conditions (Table 1). Further, the climate, morphology, and ecology of the sites and region have been previously described (Hobbie and Kling, 2014).

- The **Kuparuk River** (68.64816, -149.41152, Figure 2A) is a meandering stream flowing through primarily tundra vegetation, located about 10 km northeast of TFS. The Kuparuk River includes a long-term monitoring site for the Arctic LTER, used as a site for ecological study and monitoring since 1979. From 1983-2016, the 4th order reach of the Kuparuk River was used for a whole-stream fertilization study (Peterson et al., 1993; Slavik et al., 2004; Iannucci et al., 2021), where phosphorous (H₃PO₄) was continuously added to assess response to nutrient fertilization. As the Kuparuk River continues north, it meets a large aufeis (ice) field (Yoshikawa et al., 2007; Terry et al., 2020).
- **Oksrukuyik Creek** (68.68740, -149.095, Figure 2B) is a clear-water, low-gradient stream meandering through primarily tundra landscape, with intermittent presence of stream-lake connectivity (Shogren et al., 2019). Oksrukuyik Creek is also an Arctic LTER long-term monitoring site, approximately 20 km northeast of TFS.
- **Trevor Creek** (68.28482, -149.350063, Figure 2C) is a mountainous alpine stream, draining into the Atigun River watershed, located 30-km south of TFS. Trevor Creek drains primarily steep, rocky slopes with limited heath and willow vegetation. The majority of stream runoff is generated by precipitation and snowmelt.

As a result of long-term study and a sustained commitment to data stewardship, the Arctic LTER and TFS hosts an extensive catalogue of terrestrial, aquatic, and atmospheric data that are complementary to the data presented in this publication. For more information, please see the LTER data catalogue

(<https://arc-lter.ecosystems.mbl.edu/data-catalog>), in addition to the abiotic and biotic monitoring data from the TFS Spatial and Environmental Data Center (<https://toolik.alaska.edu/edc/index.php>).

190 **2.1.2 National Parks Service and U.S. Geological Survey Sites**

We also sampled three watersheds associated with the National Park Service (NPS) Arctic Inventory and Monitoring Network and a project funded by the U.S. Geological Survey's (USGS) Changing Arctic Ecosystem program. The Agashashok and Cutler River watersheds are within Noatak National Preserve and the Akillik River watershed is within Kobuk Valley National Park. All three watersheds
195 are situated near the northern extent of Alaska's boreal forest, where tree line is expanding (Suarez et al., 1999), and subcatchments vary in areal extent of forested versus tundra land cover. The study sites vary with respect to permafrost characteristics, including soil texture, ground ice content, and subsurface hydrology (O'Donnell et al., 2016). Evidence suggests stream chemistry varies across these watersheds, including the form, amount, and age of dissolved carbon (O'Donnell et al., 2020).

- 200 • The **Cutler River** (67.845, -158.316, Figure 3A) flows north out of the Baird Mountains through gently rolling tundra into the upper Noatak River. The watershed is underlain by ice-rich glaciolacustrine deposits (O'Donnell et al., 2016), and soils tend to be organic-rich and poorly drained. Vegetation is dominated by moist acidic tundra and wet sedge meadows.
- 205 • The **Akillik River** (67.201, -158.572, Figure 3B) flows south out of the Baird Mountains and into the Kobuk River downstream of the village of Ambler, Alaska. The river passes through alpine terrain in the headwaters before draining terrain comprised of ice-rich loess in the lower reaches. Vegetation is a mixture of boreal spruce forests and tundra.

- The **Agashashok River** (67.268, -162.636, Figure 3C) is a braided, clearwater river that flows from the northeast to southwest into the lower Noatak River north of Kotzebue, Alaska. The headwaters drain rocky, alpine tundra terrain of the western Brooks Range. Downstream, the river drains broader valleys with a mixture of boreal spruce forest and tundra vegetation. The watershed is underlain by shallow bedrock and permafrost is generally ice-poor (O'Donnell et al., 2016).

2.2 Synoptic Sampling Campaign Design

2.2.1 Arctic LTER Sites

Our sampling of the TFS watershed networks was designed to capture 30-50 “nested” subcatchments within the Kuparuk River, and Oksrukuyik and Trevor Creeks. Site selection was based primarily on (1) presence of flowing surface waters, (2) representation across varying subcatchment drainage areas, and (3) site accessibility. Often, we *a priori* chose sites located at subcatchment confluences, sampling both upstream locations and then downstream of river mixing. In each of the TFS watersheds, we performed 5 repeated synoptic campaigns, sampling each stream network in August 2016, June 2017, August 2017, June 2018, and August 2018 (exact dates in Table 2). We accessed sampling sites either on-foot or by helicopter within a 6-hour period.

2.2.2 NPS/USGS Sites

Sampling of the NPS/USGS watershed networks was designed to capture ~5-10 subcatchments within the Agashashok, Cutler, and Akillik Rivers. Sites were selected to span a gradient of size (subcatchment area, stream order), vegetation (forest vs. tundra), and permafrost characteristics (parent material, ground ice content). Due to variation in watershed aspect, streams also spanned a spatial gradient in

permafrost ground temperatures, areal extent, and active layer thickness (Panda et al., 2016; Sjöberg et al., 2021). In addition to stream chemistry parameters, stream discharge was measured, and samples were collected to characterize stream biota (benthic biofilm, macroinvertebrates, and resident juvenile fish).

In each of the NPS/USGS watersheds, we performed 4-10 repeated synoptic campaigns, sampling each stream network in June, August, and September 2015; June, August, and September 2016; June and August 2017; and June and August/September 2018 (exact dates in Table 2). We accessed sampling sites by helicopter within a 24- to 96-hour period.

3 Methods

3.1 Synoptic Site Characterization

3.1.1 Subcatchment Delineation for Drainage Area

The location of each stream sampling site was recorded in a spreadsheet and imported into GIS software (ESRI ArcGIS v. 10.4). These sites served as starting points ('pour points') from which watersheds and subcatchments were delineated following the general procedure described here:

(<https://support.esri.com/en/technical-article/000012346>). The following two digital elevation models (DEMs) were needed to cover the spatial distribution of the stream sampling sites and were used to create the necessary flow direction and flow accumulation layers: ArcticDEM from the Polar Geospatial Center (Porter et al., 2018) and ASTER GDEM v.2 (NASA/METI/AIST/Japan Spacesystems and US/Japan ASTER Science Team, 2009). A Python script was written to iterate over the list of sample sites and execute the watershed delineation procedure.

3.1.1 Estimation of terrestrial catchment characteristics for TFS sites

250 We characterized the terrestrial environment of the TFS sites using remotely sensed data pertaining to the vegetation and topography of each subcatchment. For each subcatchment polygon, we extracted the mean, standard deviation, and range of the elevation, slope, and topographic position index (i.e., the elevation of a given pixel relative to surrounding pixels, sometimes known as slope position). These metrics were calculated from 25-meter-resolution elevation data retrieved from the USGS National Map website (<https://viewer.nationalmap.gov/basic/>). The normalized difference vegetation index (NDVI), which indicates the presence of green vegetation, was derived from imagery acquired in summer 2012 by the ETM+ sensor on Landsat 7 (courtesy of the USGS). We also extracted percent cover of vegetation classes in each subcatchment from the 30-meter-resolution Jorgenson northern Alaska ecosystems map (Muller et al., 2018). All data extraction was performed using zonal statistics via
260 ArcPy (ESRI, 2016) in Python.

3.2 Water Sampling & Analysis

3.2.1 Field sample collection & preparation

3.2.1.1 Arctic LTER

During each synoptic campaign, at each site we measured *in-situ* physiochemical variables (this section)
265 and sampled stream surface water for chemical analysis (section 3.2.2). All physical water samples were “grab” sampled directly from the stream thalweg, or as close to mid-channel as could be safely accessed. We collected samples in acid-washed and triple-rinsed 1-L amber PCTE bottles. We used handheld YSI ProPlus multiparameter probes (YSI Instruments Part No: 626281) and YSI ProODO Dissolved Oxygen Meter (YSI Instruments Part No: 6050020) to measure specific conductance
270 ($\mu\text{S}/\text{cm}$), pH, temperature ($^{\circ}\text{C}$), and dissolved oxygen (DO, in % saturation and $\text{mg O}_2/\text{L}$) at each

sampling site. We placed the probe into the water column where the water sample was taken and waited for the temperature and DO readings to stabilize before recording the final value.

Upon returning to the lab at TFS, we processed each water sample into aliquots for specific analytes within 8 hours of collection. We lab-filtered samples for dissolved water chemistry and nutrients using handheld 60 mL syringes. We triple-rinsed syringes with unfiltered sample water. Then, we sparged each filter cartridge with ~10 mL of sample water prior to sample filtration; we used the sparge volume as the initial bottle rinse. We filtered samples for DOC/TDN into triple-rinsed amber 60-mL HDPE bottles using a 25 mm 0.2 μm cellulose acetate filter (Sartorius CA membrane, 11107-25-N). We filtered samples for dissolved nutrients, anions, and cations into triple-rinsed clear HDPE 60-mL bottles using a 47 mm 0.7 μm glass fiber filter (Whatman GF/F, 1825-047). Additionally, we placed ~60-mL of unfiltered sample water into a clear HDPE bottle for analysis of turbidity (NTU) and alkalinity (mg CaCO_3/L). After processing, we froze samples at -4°C until analysis, except for aliquots for DOC and total dissolved nitrogen (TDN). We stored DOC/TDN samples at 2°C until analysis. Samples were shipped express to the University of Vermont (UVM) and Brigham Young University (BYU) for further analysis.

3.2.1.2 NPS/USGS

While sample collection and processing were similar between the TFS and NPS/USGS field sites, the filtration step varied slightly. For NPS/USGS samples, we followed standard USGS protocols. We filtered all samples for nutrient, anion, and cation analysis using 0.45- μm capsule filters (Geotech Veraspor dispos-a-filter) into 250- or 500-mL HDPE bottles. We filtered samples for DOC and TDN into 125-mL amber glass bottles. Samples for alkalinity and total Fe were left unfiltered. DIC samples were collected without filtering or any headspace in 60-cc luer-lock syringes fit with two-way

stopcocks. After processing, we froze samples at -4 °C until analysis, with the exception of aliquots for DOC, TDN, and DIC that were stored at 2 °C until analysis. Samples were shipped express to Oregon
295 State University's Cooperative Chemical Analytical Laboratory (CCAL; <http://ccal.oregonstate.edu/>) or the USGS in Boulder, Colorado, for further analysis.

3.2.2 Dissolved water chemistry analysis

3.2.2.1 Arctic LTER

We include further detail on analytical methods and instrumentation in Table 3, though we briefly
300 describe our methods here. We measured DOC (as non-purgeable organic carbon, nPOC) and total dissolved nitrogen (TDN) with a total carbon analyzer (Shimadzu TOC-LCPH with a Total Nitrogen analyzer and ASI-L autosampler). We determined dissolved organic matter (DOM) optical properties including the spectral ratio (S_r , unitless) and specific ultraviolet absorbance at 254 nm ($SUVA_{254}$) from the TOC/TN dataset (Helms et al. 2008, Hansen et al. 2016). We colorimetrically analyzed SRP,
305 particulate phosphorous (PP), and total dissolved phosphorous (TDP) on a spectrophotometer (Shimadzu UV-2600). We quantified inorganic nitrogen species (nitrate, NO_3^- ; ammonium, NH_4^+) using a flow-through injection analysis (Lachat Quikchem Flow Injection Analysis System). We measured several cations (Na^+ , Li^+ , K^+ , Mg^{2+} , Ca^{2+} , NH_4^+), anions (F^- , Cl^-), oxoanions (NO_2^- , SO_4^{2-} , NO_3^- , PO_4^{3-}) and organic acids (acetate, CH_3COO^- ; and formate, $HCOO^-$) on an ion chromatography system
310 (Thermo Fisher Scientific Dionex ICS5000). We quantified other geogenic anions and cations (e.g., Al^{3+} , As^{3-} , B^{3-} , Ba^{2+} , Br^+ , Ca^{2+} , Cd^{2+} , Co^{2+} , CrO_4^- , nominally-dissolved Cu and Fe, K^+ , MoO_3^{2-} , Mg^{2+} , Mn^{2+} , Na^+ , Ni^{2+} , P, Pb^{2+} , S^{2-} , Se^{2-} , dissolved Si, Sn^{2+} , Sr^{2+} , Ti, V, Zn^{2+}) on an inductively coupled plasma mass spectrometer (ICP-MS, iCAP 7000 series, Thermo Scientific). To estimate turbidity (NTU), we used using benchtop UV-visible spectrophotometers (s::can Messtechnik GmbH, Vienna,

315 Austria). We analyzed all samples at room temperature after allowing them to thaw on a lab bench for
2-4 h prior to analysis.

3.2.2.2 NPS/USGS

We include further detail on analytical methods and instrumentation in Table 3. For the NPS/USGS
sites, we measured DOC and DIC (O.I Analytical Model 700 TOC Analyzer and Shimadzu TOC-
320 VCSH Combustion Analyzer, respectively). We characterized DOM aromaticity by measuring UV-
visible absorbance on filtered stream water samples on an Agilent Model 8453 photodiode array, and
then calculating SUVA₂₅₄ (Weishaar et al., 2003). We also measured TDN and TDP on a Technicon
Auto-Analyzer II. We quantified inorganic nitrogen species ($\text{NO}_3^- + \text{NO}_2^-$ and unionized NH_3) and
orthophosphate (PO_4^{3-}) using a flow-through injection analysis system (Lachat Quikchem 8500). We
325 calculated alkalinity using a titration to 4.5, using 0.02N Na_2CO_3 and 0.02 N H_2SO_4 (ManTech PC-
Titrate Auto Titrator System). Finally, we used ion chromatography to measure Cl^- and SO_4^{2-} (Dionex
1500 IC) and absorption spectroscopy to measure Na^+ , K^+ , Mg^{2+} , Ca^{2+} , and total Fe (Shimadzu AA-
7000).

330 3.3 Estimation of ecohydrological metrics

In addition to reporting solute concentrations for each synoptic campaign (e.g., Figures 4-5), we
estimated ecohydrological metrics for each nested site and watershed. Across these analyses, we
assigned any value below detection as the values of half the limit of quantification and kept these data
points in the analysis. When the sample was not run for a specific solute, the cell was left blank.

335 3.3.1 Subcatchment Leverage

First, we estimated *subcatchment leverage* from each of the synoptic sampling events for each solute.
Subcatchment leverage is calculated as the difference in terms of concentration at each site (C_s) from

the concentration at the watershed outlet (C_o), subcatchment area (A_s) relative to the entire watershed area (A_o), and specific discharge at the sampling location ($q = Q_s/A_s$, where Q_s and A_s are the discharge and subcatchment area at the sampling point):

$$\text{Specific Subcatchment Leverage} = \left[(C_s - C_o) * \frac{A_s}{A_o} * q \right] \quad (1)$$

In the case of Eqn. 1, leverage is expressed in units of flux (mass/volume/time). However, if specific discharge is unavailable for each sampling location leverage can be estimated using only variability in concentration and subcatchment area, so long as specific discharge (q) is similar between subcatchments (Asano et al., 2009; Karlsen et al., 2016). With the exception of the Agashashok River, which has flow generated from deeper flowpaths, our study watersheds have very little regional groundwater influence (Lecher, 2017), and the synoptic campaigns were performed near base-flow conditions. Therefore, for the purposes of this study, we assumed that q was similar for subcatchments within a study watershed, but not necessarily across the six study watersheds. This assumption was tested at all Arctic LTER sites using dilution gauging at a subset of sites in summer 2018 and 2019, where we found that values of specific discharge were similar across subcatchment sizes (Shogren, unpublished data). We used Eqn. 2 to estimate subcatchment leverage for all sampling locations across sampling events:

$$\text{Subcatchment Leverage (\%)} = 100 * \left[(C_s - C_o) * \frac{A_s}{A_o} \right] \quad (2)$$

Here, subcatchment leverage has units of concentration, or percentage when normalized to outlet concentration. In other words, the distributed mass balance is relative to a pre-determined outflow point; with the presented analysis, we used the furthest downstream point with the largest drainage area as our

“outlet” location. The interpretation of leverage values is opposite at the site and watershed scales (Abbott et al., 2018; Shogren et al., 2019). For example, a site with a positive value for subcatchment leverage is contributing more than the typical subcatchment in the watershed. Conversely, a watershed with a mean leverage value that is positive is indicative of a net removal in the stream network because there is more solute in the tributaries than can be accounted for at the watershed outlet, while a negative value suggests solute production in the network (Abbott et al., 2018; Shogren et al., 2019). We report both mean leverages for each catchment (presented in Figures 6 and 7) and site-specific subcatchment leverages for each solute (Figure 10 for DOC and NO_3^- , but all other solutes can be found within the ecohydrological metrics datasets).

3.3.2 Concentration Variance Collapse

Next, to assess the representative “patch” size where concentration variance is reduced, we determined the threshold of concentration *variance collapse* for each solute from each synoptic sampling event (shown in Figure 8). Using concentrations plotted over watershed area, we used the ‘changepoint’ package in R (Killick and Eckley, 2014) to determine the collapse in variance of concentration across the whole watershed area. To determine the reduction in variance statistically, we used the pruned exact linear time (PELT) method, which compares differences in data points to determine statistical breakpoints (Abbott et al., 2018; Shogren et al., 2019). We performed this analysis using scaled concentrations, which were scaled by subtracting the whole watershed mean and dividing by the standard deviation to facilitate comparison of changes in variance and evaluate convergence towards the watershed mean. The variance collapse threshold is therefore expressed in units of area (here as km^2). A non-significant variance collapse threshold can be interpreted to mean either the processes controlling

lateral fluxes are operating at too small or too large of a scale to be captured using a subcatchment
380 sampling approach.

3.3.3 Spatial Persistence

Lastly, we analyzed this spatially rich synoptic data to quantify the *spatial persistence* of stream
nutrient concentrations and to determine the level of sub-grid resolution necessary to represent controls
on lateral nutrient loss. The spatial persistence metric indicates whether spatial sampling is
385 representative or whether spatial patterns “reshuffle” over time. Spatial persistence (r_s) is calculated as:

$$(r_s) = \left(\frac{\text{covariance}(rg_x, rg_y)}{\sigma_{rg_x} \sigma_{rg_y}} \right) \quad (3)$$

Where rg_x is the rank of subcatchments at the time of synoptic sampling, rg_y is the rank of the long-term
flow weighted concentrations, while σ_{rg_x} and σ_{rg_y} are the standard deviation of the rank variables. We
calculated spatial persistence using the correlation function in R (Version 3.3.0), using the Spearman
390 method (Abbott et al., 2018; Shogren et al., 2019). Significance was tested using a student’s t
distribution test. Additional methods for calculating spatial persistence have now been proposed that do
not require discharge data for the flow weighting (Gu et al., 2021). For the purposes of the Arctic LTER
analysis, we estimated spatial persistence as the Spearman’s correlation between Early (June) and Late
(August) site concentrations, resulting in a single spatial persistence metric (r_s) for 2017 and 2018. For
395 the NPS/USGS sites, spatial persistence was calculated as the correlation between site locations
sampled in the Early (June) and Mid (July) and the Mid to Late (August or September) seasons.

3.4 Use and interpretation of ecohydrological ecosystem metrics

The original intent of this manuscript was to present our unique Arctic datasets and showcase the utility
of a synoptic framework in combination with metrics that describe the spatial distribution of river

400 chemistry. To further highlight how these metrics can inform future sampling design and address fundamental ecological questions, below we describe patterns for DOC and NO_3^- in the TFS watersheds.

For solutes, the spatial variability in concentration depends on the strength and connectivity of both source and sink patches superimposed on the structure of the stream network (Abbott et al., 2018). When we plot solute concentration against subcatchment area, we find more variability water chemistry
405 in smaller subcatchments ($<30 \text{ km}^2$). This can be interpreted as a spatial “fingerprint” and is shown most clearly in Figure 10, which displays the spatial distribution of DOC and NO_3^- concentrations across watersheds and sampling campaigns. Generally high concentration variability in smaller headwaters, which converges to mean watershed behaviour towards the catchment outlet holds with the conceptualizations of large rivers as “chemostats” (Creed et al., 2015). In the context of Arctic
410 watersheds, these concentration/area relationships reveal consistently high DOC and low NO_3^- concentrations in the low-gradient tundra watersheds (Kuparuk River and Oksrukuyik Creek), despite high variability in smaller contributing subcatchments. In contrast, the alpine watershed Trevor Creek, has relatively low DOC and high NO_3^- concentrations, likely due to shorter and faster hydrologic flowpaths and lower terrestrial biomass (Shogren et al., 2019). Overall, these findings are consistent
415 with studies that indicate that slower, longer flowpaths and productive terrestrial vegetation control carbon and nutrient transfer and mobilization in lower-gradient tundra watersheds (Shogren et al., 2019, 2021). If we assume that spatial variability in stream network water chemistry depends primarily on the extent and connectivity of upstream sources/sinks, then the patches sizes that control solute fluxes can be assessed by the spatial scale of the variance collapse (Abbott et al., 2018; Shogren et al., 2019).
420 Across all three TFS watersheds, the generality of variance collapse at intermediate scales is indicative

that subcatchment scale “patches” (~10-50 km²) control whether carbon and inorganic nitrogen is produced or removed at the watershed scale (Figure 10). In addition, the consistency of the thresholds across sampling campaigns (Figure 8 and 10) highlights the importance of capturing intermediate scale biogeochemistry to bridge understandings from plot-level experimentation to larger more regional-scale observations (Shogren et al. 2019).

When we convert concentrations into estimates of subcatchment leverage (e.g., Figure 6, 7, 10 and Figure 11), patterns emerge that further contextualize the spatial distribution of DOC and NO₃⁻ concentrations. First, we can investigate whole watershed (“net”) behaviour by calculating the mean leverage and examining the distribution of values with boxplots (as in Figures 6 and 7). As a more specific example, mean NO₃⁻ leverage within the Kuparuk watershed (Figure 6D, second row) were consistently above zero (note the reversed axis), revealing strong removal or retention before it reached the watershed outlet, which is consistent with high biotic N demand. Within this same watershed, DOC leverage values were often at or just above the zero line (Figure 6D, first row), representing primarily conservative transport of DOC (i.e., no net production or uptake). Within the lake-influenced Oksrukuyik watershed, NO₃⁻ leverage values were more variable (i.e., leverage above/below zero-line; Figure 6E, second row), implying a combination of removal and production mechanisms acting across the watershed network. When visualized as “net” behaviour, the watershed and season-dependent directionality of net leverage patterns are congruent with emerging evidence that landscape template exerts strong control on biogeochemical signals in Arctic rivers (Vonk et al., 2019; Tank et al., 2020; Shogren et al., 2021). As a compliment to the first approach, we can additionally examine individual subcatchment leverage values to reveal the effect of each contribution on what we observe at the

watershed outlet. This can be interpreted similarly to statistical leverage, where one or more points may exert high influence on a linear regression.

Across all TFS watersheds, there are a few select subcatchments that contribute
445 disproportionately to DOC fluxes, while the more variable patterns for NO_3^- suggest additional spatial and seasonal controls (Figure 11). For example, patterns in the Kuparuk River and Oksrukuyik Creek (Figure 11a-b) could be interpreted to mean that DOC is transported conservatively in lower gradient landscapes, while lateral fluxes of NO_3^- are more tightly controlled by biotic demand (Harms et al., 2016; Khosh et al., 2017; Connolly et al., 2018; Kendrick et al., 2018; Iannucci et al., 2021). Across
450 solutes and watersheds, the information gleaned from the leverage metric is useful in several ways. First, subcatchment leverages allow for the direct identification of watershed areas that are disproportionately driving carbon and nutrient exports. For any chosen solute or suite of materials, sites identified as “high leverage” indicate strong source/sink behaviour, which could be (1) validated with regular field observations that relate riparian or terrestrial conditions with empirical measurements of
455 water chemistry, (2) selected for further study designed to identify the abiotic and biotic mechanisms that drive patterns of riverine chemistry, and/or (3) identified as non-representative sites relative to proximal subcatchments of similar size and terrestrial characteristics. Relatedly, estimating subcatchment leverage enables researchers to identify sites that are representative of watershed-scale behaviour, which could be used to more effectively scale biogeochemical dynamics in Arctic rivers
460 relative to outlying subcatchments (Kicklighter et al., 2013; Pinay et al., 2015; Aguilera et al., 2013).

Finally, the application of the simple spatial persistence metric can help researchers determine whether a sampling location is behaving consistently, or if solute contributions are moving in space

across sampling events (Abbott et al., 2018; Dupas et al., 2019). In the context of work in remote watersheds, the ability for researchers to identify both stable and unstable processes presents an exciting opportunity to ask questions about the consistency of subcatchment contributions and optimize sampling or experimental design. For example, DOC concentrations are generally spatially stable between early and late sampling events ($r_s > 0.50$), particularly in the Kuparuk River and Trevor Creek watersheds (Figure 9). In these landscapes, a high rank correlation indicates that repeated sampling of the same location will result in a similar spatial distribution of concentrations. While sampling repeatedly in the early and late seasons may reveal increases or decreases in solute concentrations (Shogren et al. 2019), the high degree of relatedness indicates that these patterns will be maintained across the watershed network. However, the low persistence ($r_s < 0.50$) for DOC in the Oksrukuyik Creek watersheds signifies substantial spatial shifts across the early and late thaw season (Shogren et al. 2019). While there was variability in the persistence across watersheds and solutes, the stability metric can be used by future researchers to identify whether sampling the same location repeatedly does or does not represent the spatial dynamics across sampling events.

4. Data Availability

The data from the NPS/USGS are available at <https://doi.org/10.5066/P9SBK2DZ> (O'Donnell et al., 2021). Data from TFS are stored at the Environmental Data Center data repository (<http://dx.doi.org/10.6073/pasta/258a44fb9055163dd4dd4371b9dce945>) (Abbott et al., 2021a).

5. Conclusions

With this work, we provide a detailed characterization of physical, chemical, and biological parameters that are essential to using river network chemistry to infer ecosystem-level carbon and nutrient balance.

We apply novel metrics to these data that describe the spatiotemporal patterns of watershed

485 biogeochemistry in six permafrost-underlain Arctic watersheds. These data represent a high-resolution and temporally replicated river chemistry dataset from understudied permafrost-dominated regions.

Combining these measures with remotely sensed data, plot-level experiments, and numerical models could advance our understanding of permafrost ecosystems in the face of climate change and other disturbance.

490

Author contributions: All co-authors participated in the field collection, laboratory analysis, and/or curation of the dataset, and contributed to writing and/or editing this paper. AJS was primarily responsible for writing this paper and assembly of the archival database.

495 **Competing Interests:** The authors declare that they have no conflict of interest.

Acknowledgements: Data and facilities were provided by the Arctic LTER at TFS, NPS, and USFS.

The authors gratefully acknowledge the Arctic LTER, TFS staff, and CH2M HILL Polar Services for assistance in support of this work. The authors also thank the National Park Service's Western Arctic

500 Parklands in Kotzebue, Alaska, for assisting with logistics and permitting. DEMs were provided by the Polar Geospatial Center under NSF-OPP awards 1043681, 1559691, and 1542736.

Financial Support: The authors would also like to acknowledge their funding support: AJS (NSF-DBI-1906381, NSF-OPP-1916567); JPZ and TW (NSF-EAR-1846855, NSF-OPP-1916567); BWA (NSF-505 OPP-1916565), WBB (NSF-OPP-1916576, NSF DEB-1637459); and FI and AM (NSF DEB-1637459). This work was supported by the Changing Arctic Ecosystems Initiative of the Wildlife program of the USGS Ecosystems Mission Area. Additional support was provided by the NPS Arctic Inventory & Monitoring program. Any use of trade, firm, or product names is for descriptive purposes only and does not imply endorsement by the U.S. Government.

510

References

- Abbott, B. W., Jones, J. B., Godsey, S. E., Larouche, J. R., and Bowden, W. B.: Patterns and persistence of hydrologic carbon and nutrient export from collapsing upland permafrost, *Biogeosciences*, 12, 3725–3740, <https://doi.org/10.5194/bg-12-3725-2015>, 2015.
- Abbott, B. W., Baranov, V., Mendoza-Lera, C., Nikolakopoulou, M., Harjung, A., Kolbe, T., Balasubramanian, M. N., Vaessen, T. N., Ciocca, F., Campeau, A., Wallin, M. B., Romeijn, P., Antonelli, M., Gonçalves, J., Datry, T., Laverman, A. M., de Dreuzy, J.-R., Hannah, D. M., Krause, S., Oldham, C., and Pinay, G.: Using multi-tracer inference to move beyond single-catchment ecohydrology, *Earth-Science Reviews*, 160, 19–42, <https://doi.org/10.1016/j.earscirev.2016.06.014>, 2016.
- Abbott, B. W., Pinay, G., and Burt, T. P.: Protecting Water Resources Through a Focus on Headwater Streams, EO076897, <https://doi.org/10.1029/2017EO076897>, 2017.
- Abbott, B. W., Gruau, G., Zarnetske, J. P., Moatar, F., Barbe, L., Thomas, Z., Fovet, O., Kolbe, T., Gu, S., Pierson-Wickmann, A.-C., Davy, P., and Pinay, G.: Unexpected spatial stability of water chemistry in headwater stream networks, 21, 296–308, <https://doi.org/10.1111/ele.12897>, 2018.
- Abbott, B. W., Zarnetske, J. P., Bowden, W. B., and Shogren, A. J.: Repeated synoptic watershed chemistry from three watersheds near Toolik Field Station, Alaska, summer 2016-2018, Arctic LTER, Environmental Data Initiative, 2021a.
- Abbott, B. W., Rocha, A. V., Shogren, A., Zarnetske, J. P., Iannucci, F., Bowden, W. B., Bratsman, S. P., Patch, L., Watts, R., Fulweber, R., Frei, R. J., Huebner, A. M., Ludwig, S. M., Carling, G. T., and O'Donnell, J. A.: Tundra wildfire triggers sustained lateral nutrient loss in Alaskan Arctic, 27, 1408–1430, <https://doi.org/10.1111/gcb.15507>, 2021b.
- Aguilera, R., Marcé, R., and Sabater, S.: Modeling nutrient retention at the watershed scale: Does small stream research apply to the whole river network?: NUTRIENT RETENTION IN IMPAIRED RIVERS, 118, 728–740, <https://doi.org/10.1002/jgrg.20062>, 2013.
- Appling, A. P., Hall, R. O., Yackulic, C. B., and Arroita, M.: Overcoming Equifinality: Leveraging Long Time Series for Stream Metabolism Estimation, 123, 624–645, <https://doi.org/10.1002/2017JG004140>, 2018.
- Asano, Y., Uchida, T., Mimasu, Y., and Ohte, N.: Spatial patterns of stream solute concentrations in a steep mountainous catchment with a homogeneous landscape, 45, <https://doi.org/10.1029/2008WR007466>, 2009.
- Bernhardt, E. S., Blaszczyk, J. R., Ficken, C. D., Fork, M. L., Kaiser, K. E., and Seybold, E. C.: Control Points in Ecosystems: Moving Beyond the Hot Spot Hot Moment Concept, 20, 665–682, <https://doi.org/10.1007/s10021-016-0103-y>, 2017.
- Bowden, W. B.: CSASN Channel Nutrients from 2010 to 2012 in I8 Inlet, I8 Outlet, Peat Inlet and Kuparuk Rivers, <http://dx.doi.org/10.6073/pasta/d19adb5a8fe01f67806e5afccf283b52>, 2013.
- Bring, A., Fedorova, I., Dibike, Y., Hinzman, L., Mård, J., Mernild, S. H., Prowse, T., Semenova, O., Stuefer, S. L., and Woo, M.-K.: Arctic terrestrial hydrology: A synthesis of processes, regional effects, and research challenges, 121, 621–649, <https://doi.org/10.1002/2015JG003131>, 2016.
- Burns, D. A., Pellerin, B. A., Miller, M. P., Capel, P. D., Tesoriero, A. J., and Duncan, J. M.: Monitoring the riverine pulse: Applying high-frequency nitrate data to advance integrative understanding of biogeochemical and hydrological processes, e1348, <https://doi.org/10.1002/wat2.1348>, 2019.
- Burt, T. P. and Pinay, G.: Linking hydrology and biogeochemistry in complex landscapes, *Progress in Physical Geography*, 29, 297–316, <https://doi.org/10.1191/0309133305pp450ra>, 2005.

- 550 Byrne, P., Runkel, R. L., and Walton-Day, K.: Synoptic sampling and principal components analysis to identify sources of water and metals to an acid mine drainage stream, *Environ Sci Pollut Res*, 24, 17220–17240, <https://doi.org/10.1007/s11356-017-9038-x>, 2017.
- Collier, N., Hoffman, F. M., Lawrence, D. M., Keppel-Aleks, G., Koven, C. D., Riley, W. J., Mu, M., and Randerson, J. T.: The International Land Model Benchmarking (ILAMB) System: Design, Theory, and Implementation, 10, 2731–2754, <https://doi.org/10.1029/2018MS001354>, 2018.
- 555 Connolly, C. T., Khosh, M. S., Burkart, G. A., Douglas, T. A., Holmes, R. M., Jacobson, A. D., Tank, S. E., and McClelland, J. W.: Watershed slope as a predictor of fluvial dissolved organic matter and nitrate concentrations across geographical space and catchment size in the Arctic, 13, 104015–104015, <https://doi.org/10.1088/1748-9326/aae35d>, 2018.
- Covino, T.: Hydrologic connectivity as a framework for understanding biogeochemical flux through watersheds and along fluvial networks, *Geomorphology*, 277, 133–144, <https://doi.org/10.1016/j.geomorph.2016.09.030>, 2017.
- 560 Creed, I. F., McKnight, D. M., Pellerin, B. A., Green, M. B., Bergamaschi, B. A., Aiken, G. R., Burns, D. A., Findlay, S. E. G., Shanley, J. B., Striegl, R. G., Aulenbach, B. T., Clow, D. W., Laudon, H., McGlynn, B. L., McGuire, K. J., Smith, R. A., and Stackpoole, S. M.: The river as a chemostat: fresh perspectives on dissolved organic matter flowing down the river continuum, *Can. J. Fish. Aquat. Sci.*, 72, 1272–1285, <https://doi.org/10.1139/cjfas-2014-0400>, 2015.
- 565 Docherty, C. L., Riis, T., Hannah, D. M., Rosenhøj Leth, S., and Milner, A. M.: Nutrient uptake controls and limitation dynamics in north-east Greenland streams, 37, 1440107–1440107, <https://doi.org/10.1080/17518369.2018.1440107>, 2018.
- Dupas, R., Minaudo, C., and Abbott, B. W.: Stability of spatial patterns in water chemistry across temperate ecoregions, *Environ. Res. Lett.*, 14, 074015, <https://doi.org/10.1088/1748-9326/ab24f4>, 2019.
- 570 Farquharson, L. M., Romanovsky, V. E., Cable, W. L., Walker, D. A., Kokelj, S., and Nicolsky, D.: Climate change drives widespread and rapid thermokarst development in very cold permafrost in the Canadian High Arctic, *Geophys. Res. Lett.*, 2019GL082187, <https://doi.org/10.1029/2019GL082187>, 2019.
- Frei, R. J., Abbott, B. W., Dupas, R., Gu, S., Gruau, G., Thomas, Z., Kolbe, T., Aquilina, L., Labasque, T., Laverman, A., Fovet, O., Moatar, F., and Pinay, G.: Predicting Nutrient Incontinence in the Anthropocene at Watershed Scales, *Front. Environ. Sci.*, 7, <https://doi.org/10.3389/fenvs.2019.00200>, 2020.
- 575 Gao, T., Zhang, Y., Kang, S., Abbott, B. W., Wang, X., Zhang, T., Yi, S., and Gustafsson, O.: Accelerating permafrost collapse on the Eastern Tibetan Plateau, *Environ. Res. Lett.*, <https://doi.org/10.1088/1748-9326/abf7f0>, 2021.
- Gardner, K. K. and McGlynn, B. L.: Seasonality in spatial variability and influence of land use/land cover and watershed characteristics on stream water nitrate concentrations in a developing watershed in the Rocky Mountain West, 45, <https://doi.org/10.1029/2008WR007029>, 2009.
- 580 Gu, S., Casquin, A., Dupas, R., Abbott, B. W., Petitjean, P., Durand, P., and Gruau, G.: Spatial Persistence of Water Chemistry Patterns Across Flow Conditions in a Mesoscale Agricultural Catchment, 57, e2020WR029053, <https://doi.org/10.1029/2020WR029053>, 2021.
- Harms, T. K., Edmonds, J. W., Genet, H., Creed, I. F., Aldred, D., Balsler, A., and Jones, J. B.: Catchment influence on nitrate and dissolved organic matter in Alaskan streams across a latitudinal gradient, 121, 350–369, <https://doi.org/10.1002/2015JG003201>, 2016.

- 585 Helton, A. M., Poole, G. C., Payn, R. A., Izurieta, C., and Stanford, J. A.: Scaling flow path processes to fluvial landscapes: An integrated field and model assessment of temperature and dissolved oxygen dynamics in a river-floodplain-aquifer system, 117, <https://doi.org/10.1029/2012JG002025>, 2012.
- Hobbie, J. E. and Kling, G. W. (Eds.): *Alaska's Changing Arctic*, Oxford University Press, <https://doi.org/10.1093/acprof:osobl/9780199860401.001.0001>, 2014.
- 590 Hoffman, F. M., Kumar, J., Mills, R. T., and Hargrove, W. W.: Representativeness-based sampling network design for the State of Alaska, 28, 1567–1586, 2013.
- Iannucci, F. M., Beneš, J., Medvedeff, A., and Bowden, W. B.: Biogeochemical responses over 37 years to manipulation of phosphorus concentrations in an Arctic river: The Upper Kuparuk River Experiment, 35, e14075, <https://doi.org/10.1002/hyp.14075>, 2021.
- 595 Kareiva, P. and Andersen, M.: *Spatial Aspects of Species Interactions: the Wedding of Models and Experiments*, Springer, Berlin, Heidelberg, 35–50, https://doi.org/10.1007/978-3-642-85936-6_4, 1988.
- Karlsen, R. H., Grabs, T., Bishop, K., Buffam, I., Laudon, H., and Seibert, J.: Landscape controls on spatiotemporal discharge variability in a boreal catchment, 52, 6541–6556, <https://doi.org/10.1002/2016WR019186>, 2016.
- 600 Keller, K., Blum, J. D., and Kling, G. W.: Geochemistry of soils and streams on surfaces of varying ages in arctic Alaska, 39, 84–98, [https://doi.org/10.1657/1523-0430\(2007\)39\[84:GOSASO\]2.0.CO;2](https://doi.org/10.1657/1523-0430(2007)39[84:GOSASO]2.0.CO;2), 2007.
- Kendrick, M. R., Huryn, A. D., Bowden, W. B., Deegan, L. A., Findlay, R. H., Hershey, A. E., Peterson, B. J., Beneš, J. P., and Schuett, E. B.: Linking permafrost thaw to shifting biogeochemistry and food web resources in an arctic river, 24, 5738–5750, <https://doi.org/10.1111/gcb.14448>, 2018.
- 605 Khamis, K., Blaen, P. J., Comer-Warner, S., Hannah, D. M., MacKenzie, A. R., and Krause, S.: High-Frequency Monitoring Reveals Multiple Frequencies of Nitrogen and Carbon Mass Balance Dynamics in a Headwater Stream, *Front. Water*, 3, 668924, <https://doi.org/10.3389/frwa.2021.668924>, 2021.
- Khosh, M. S., McClelland, J. W., Jacobson, A. D., Douglas, T. A., Barker, A. J., and Lehn, G. O.: Seasonality of dissolved nitrogen from spring melt to fall freezeup in Alaskan Arctic tundra and mountain streams, 122, 1718–1737, <https://doi.org/10.1002/2016JG003377>, 2017.
- 610 Kicklighter, D. W., Hayes, D. J., McClelland, J. W., Peterson, B. J., McGuire, A. D., and Melillo, J. M.: Insights and issues with simulating terrestrial DOC loading of Arctic river networks, 23, 1817–1836, <https://doi.org/10.1890/11-1050.1>, 2013.
- Killick, R. and Eckley, I. A.: *changepoint: An R Package for Changepoint Analysis.*, 58, 1–19, 2014.
- 615 Kling, G. W., Kipphut, G. W., Miller, M. M., and O'Brien, W. John.: Integration of lakes and streams in a landscape perspective: the importance of material processing on spatial patterns and temporal coherence, *Freshwater Biol*, 43, 477–497, <https://doi.org/10.1046/j.1365-2427.2000.00515.x>, 2000.
- Kolbe, T., Dreuzy, J.-R. de, Abbott, B. W., Aquilina, L., Babey, T., Green, C. T., Fleckenstein, J. H., Labasque, T., Laverman, A. M., Marçais, J., Peiffer, S., Thomas, Z., and Pinay, G.: Stratification of reactivity determines nitrate removal in groundwater, *PNAS*, 201816892, <https://doi.org/10.1073/pnas.1816892116>, 2019.

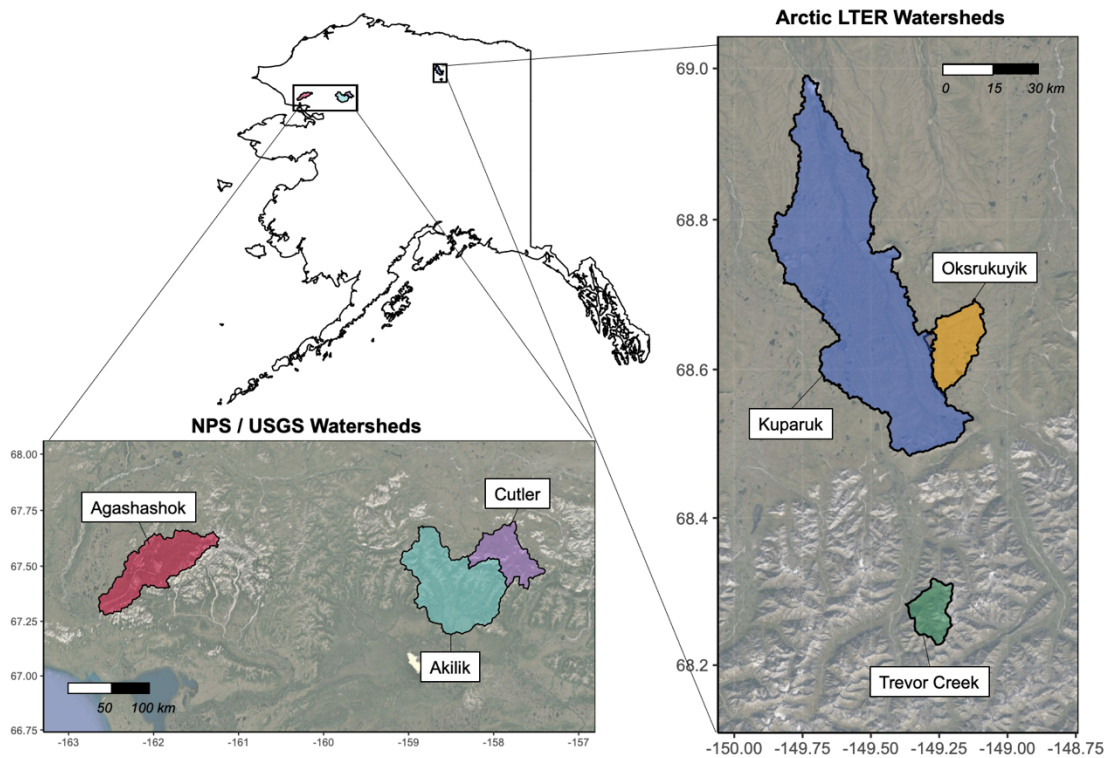
- 620 Koven, C. D., Lawrence, D. M., and Riley, W. J.: Permafrost carbon–climate feedback is sensitive to deep soil carbon decomposability but not deep soil nitrogen dynamics, *PNAS*, 112, 3752–3757, <https://doi.org/10.1073/pnas.1415123112>, 2015.
- Lamhonwah, D., Lafreniere, M. J., Lamoureux, S. F., and Wolfe, B. B.: Evaluating the hydrological and hydrochemical responses of a High Arctic catchment during an exceptionally warm summer, *Hydrol. Process.*, n/a-n/a, <https://doi.org/10.1002/hyp.11191>, 2017.
- 625 Laudon, H., Spence, C., Buttle, J., Carey, S. K., McDonnell, J. J., McNamara, J. P., Soulsby, C., and Tetzlaff, D.: Save northern high-latitude catchments, 10, 324–325, <https://doi.org/10.1038/ngeo2947>, 2017.
- Lecher, A.: Groundwater Discharge in the Arctic: A Review of Studies and Implications for Biogeochemistry, 4, 41, <https://doi.org/10.3390/hydrology4030041>, 2017.
- 630 McClelland, J. W., Déry, S. J., Peterson, B. J., Holmes, R. M., and Wood, E. F.: A pan-arctic evaluation of changes in river discharge during the latter half of the 20th century, 33, L06715, <https://doi.org/10.1029/2006GL025753>, 2006.
- McClelland, J. W., Stieglitz, M., Pan, F., Holmes, R. M., and Peterson, B. J.: Recent changes in nitrate and dissolved organic carbon export from the upper Kuparuk River, North Slope, Alaska, 112, <https://doi.org/10.1029/2006JG000371>, 2007.
- 635 McDonnell, J. J., Sivapalan, M., Vaché, K., Dunn, S., Grant, G., Haggerty, R., Hinz, C., Hooper, R., Kirchner, J. W., Roderick, M. L., Selker, J., and Weiler, M.: Moving beyond heterogeneity and process complexity: A new vision for watershed hydrology, 43, <https://doi.org/10.1029/2006WR005467>, 2007.
- McGuire, K. J., Torgersen, C. E., Likens, G. E., Buso, D. C., Lowe, W. H., and Bailey, S. W.: Network analysis reveals multiscale controls on streamwater chemistry, *PNAS*, 111, 7030–7035, <https://doi.org/10.1073/pnas.1404820111>, 2014.
- 640 Moatar, F., Abbott, B. W., Minaudo, C., Curie, F., and Pinay, G.: Elemental properties, hydrology, and biology interact to shape concentration-discharge curves for carbon, nutrients, sediment, and major ions, *Water Resour. Res.*, 53, 1270–1287, <https://doi.org/10.1002/2016WR019635>, 2017.
- Mu, C., Abbott, B. W., Norris, A. J., Mu, M., Fan, C., Chen, X., Jia, L., Yang, R., Zhang, T., Wang, K., Peng, X., Wu, Q., Guggenberger, G., and Wu, X.: The status and stability of permafrost carbon on the Tibetan Plateau, *Earth-Science Reviews*, 211, 103433, <https://doi.org/10.1016/j.earscirev.2020.103433>, 2020.
- 645 Muller, S., Walker, D. A., and Jorgenson, M. T.: Land Cover and Ecosystem Map Collection for Northern Alaska., <https://doi.org/10.3334/ORNLDAAAC/1359>, 2018.
- NASA/METI/AIST/Japan Spacesystems and US/Japan ASTER Science Team: ASTER Global Digital Elevation Model [data set], <https://doi.org/10.5067/ASTER/ASTGTM.002>, 2009.
- Newman, E. A., Kennedy, M. C., Falk, D. A., and McKenzie, D.: Scaling and Complexity in Landscape Ecology, *Front. Ecol. Evol.*, 0, <https://doi.org/10.3389/fevo.2019.00293>, 2019.
- 650 O’Donnell, J. A., Aiken, G. R., Swanson, D. K., Panda, S., Butler, K. D., and Baltensperger, A. P.: Dissolved organic matter composition of Arctic rivers: Linking permafrost and parent material to riverine carbon, 30, 1811–1826, <https://doi.org/10.1002/2016GB005482>, 2016.

- 655 O'Donnell, J. A., Carey, M. P., Koch, J. C., Xu, X., Poulin, B. A., Walker, J., and Zimmerman, C. E.: Permafrost Hydrology Drives the Assimilation of Old Carbon by Stream Food Webs in the Arctic, *Ecosystems*, 23, 435–453, <https://doi.org/10.1007/s10021-019-00413-6>, 2020.
- O'Donnell, J. A., Koch, J. C., Carey, M. P., and Poulin, B.: Stream water chemistry from Arctic Network Parks, Alaska, 2015 to 2019, U.S. Geological Survey, 2021.
- Panda, S., Romanovsky, V., and Marchenk, S.: High-resolution permafrost modeling in the Arctic Network National Parks, Preserves, & Monuments., National Park Service, Fort Collins, Colorado., 2016.
- 660 Peterson, B. J., Deegan, L., Helfrich, J., Hobbie, J. E., Hullar, M., Moller, B., Ford, T. E., Hershey, A., Hiltner, A., Kipphut, G., Lock, M. A., Fiebig, D. M., McKinley, V., Miller, M. C., Vestal, J. R., Ventullo, R., and Volk, G.: Biological Responses of a Tundra River to Fertilization, 74, 653–672, <https://doi.org/10.2307/1940794>, 1993.
- 665 Pinay, G., Peiffer, S., De Dreuzuy, J.-R., Krause, S., Hannah, D. M., Fleckenstein, J. H., Sebilo, M., Bishop, K., and Hubert-Moy, L.: Upscaling Nitrogen Removal Capacity from Local Hotspots to Low Stream Orders' Drainage Basins, 18, 1101–1120, <https://doi.org/10.1007/s10021-015-9878-5>, 2015.
- Porter, C., Morin, P., Howat, I., Noh, M.-J., Bates, B., Peterman, K., Keeseey, S., Schlenk, M., Gardiner, J., Tomko, K., Willis, M., Kelleher, C., Cloutier, M., Husby, E., Foga, S., Nakumura, H., Platson, M., Wethington, M., Williamson, C., Bauer, G., Enos, J., Arnold, G., William, K., Becker, P., Doshi, A., D'Souza, C., Cummens, P., Laurier, F., and Bojezen, M.: Arctic DEM, <https://doi.org/10.7910/DVN/OHHUKH>, 2018.
- 670 Prager, C. M., Naeem, S., Boelman, N. T., Eitel, J. U. H. H., Greaves, H. E., Heskell, M. A., Magney, T. S., Menge, D. N. L., Vierling, L. A., and Griffin, K. L.: A gradient of nutrient enrichment reveals nonlinear impacts of fertilization on Arctic plant diversity and ecosystem function, 7, 2449–2460, <https://doi.org/10.1002/ece3.2863>, 2017.
- 675 Rodríguez-Cardona, B. M., Coble, A. A., Wymore, A. S., Kolosov, R., Podgorski, D. C., Zito, P., Spencer, R. G. M., Prokushkin, A. S., and McDowell, W. H.: Wildfires lead to decreased carbon and increased nitrogen concentrations in upland arctic streams, 10, 8722, <https://doi.org/10.1038/s41598-020-65520-0>, 2020.
- Ruhala, S. S. and Zarnetske, J. P.: Using in-situ optical sensors to study dissolved organic carbon dynamics of streams and watersheds: A review, *Science of The Total Environment*, 575, 713–723, <https://doi.org/10.1016/j.scitotenv.2016.09.113>, 2017.
- 680 Schuur, E. A. G., McGuire, A. D., Schädel, C., Grosse, G., Harden, J. W., Hayes, D. J., Hugelius, G., Koven, C. D., Kuhry, P., Lawrence, D. M., Natali, S. M., Olefeldt, D., Romanovsky, V. E., Schaefer, K., Turetsky, M. R., Treat, C. C., and Vonk, J. E.: Climate change and the permafrost carbon feedback, 520, 171–179, <https://doi.org/10.1038/nature14338>, 2015.
- Shiklomanov, A. N., Bradley, B. A., Dahlin, K. M., Fox, A. M., Gough, C. M., Hoffman, F. M., Middleton, E. M., Serbin, S. P., Smallman, L., and Smith, W. K.: Enhancing global change experiments through integration of remote-sensing techniques, 17, 215–224, <https://doi.org/10.1002/fee.2031>, 2019.
- 685 Shogren, A. J., Zarnetske, J. P., Abbott, B. W., Iannucci, F., Frei, R. J., Griffin, N. A., and Bowden, W. B.: Revealing biogeochemical signatures of Arctic landscapes with river chemistry, *Sci Rep*, 9, 1–11, <https://doi.org/10.1038/s41598-019-49296-6>, 2019.
- 690 Shogren, A. J., Zarnetske, J. P., Abbott, B. W., Iannucci, F., and Bowden, W. B.: We cannot shrug off the shoulder seasons: Addressing knowledge and data gaps in an Arctic Headwater, *Environ. Res. Lett.*, <https://doi.org/10.1088/1748-9326/ab9d3c>, 2020.

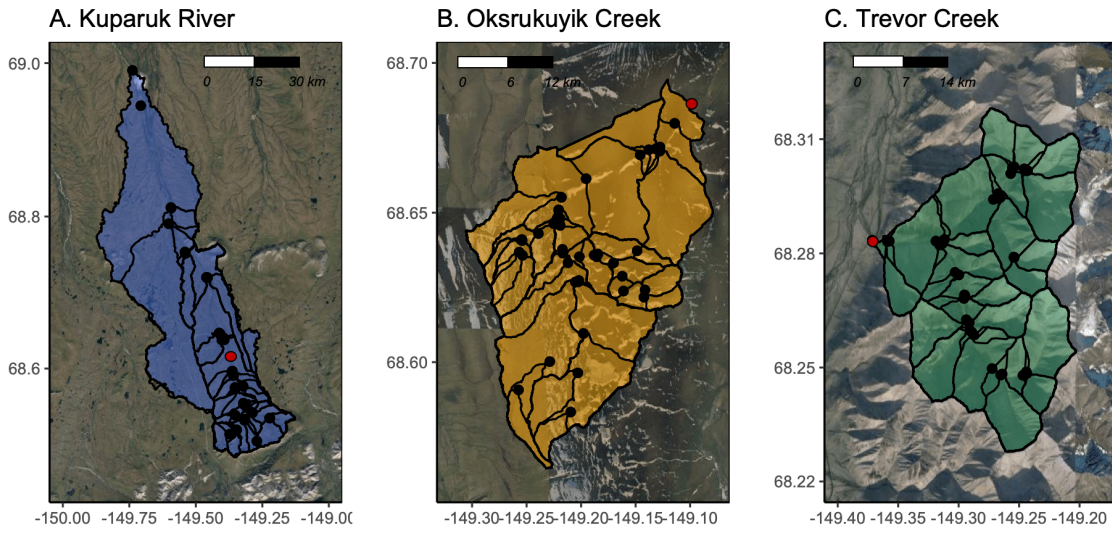
- Shogren, A. J., Zarnetske, J. P., Abbott, B. W., Iannucci, F., Medvedeff, A., Cairns, S., Duda, M. J., and Bowden, W. B.: Arctic concentration–discharge relationships for dissolved organic carbon and nitrate vary with landscape and season, *n/a*, <https://doi.org/10.1002/Ino.11682>, 2021.
- 695 Sivapalan, M.: Process complexity at hillslope scale, process simplicity at the watershed scale: is there a connection?, *17*, 1037–1041, <https://doi.org/10.1002/hyp.5109>, 2003.
- Sjöberg, Y., Jan, A., Painter, S. L., Coon, E. T., Carey, M. P., O’Donnell, J. A., and Koch, J. C.: Permafrost Promotes Shallow Groundwater Flow and Warmer Headwater Streams, *57*, e2020WR027463, <https://doi.org/10.1029/2020WR027463>, 2021.
- Slavik, K., Peterson, B. J., Deegan, L. A., Bowden, W. B., Hershey, A. E., and Hobbie, J. E.: Long-Term Responses of the Kuparuk River Ecosystem to Phosphorus Fertilization, *85*, 939–954, <https://doi.org/10.1890/02-4039>, 2004.
- 700 Suarez, F., Binkley, D., Kaye, M. W., and Stottlemyer, R.: Expansion of forest stands into tundra in the Noatak National Preserve, northwest Alaska, *6*, 465–470, <https://doi.org/10.1080/11956860.1999.11682538>, 1999.
- Tank, S. E., Striegl, R. G., McClelland, J. W., and Kokelj, S. V.: Multi-decadal increases in dissolved organic carbon and alkalinity flux from the Mackenzie drainage basin to the Arctic Ocean, *11*, 054015, <https://doi.org/10.1088/1748-9326/11/5/054015>, 2016.
- 705 Tank, S. E., Vonk, J. E., Walvoord, M. A., McClelland, J. W., Laurion, I., and Abbott, B. W.: Landscape matters: Predicting the biogeochemical effects of permafrost thaw on aquatic networks with a state factor approach, 1–13, <https://doi.org/10.1002/ppp.2057>, 2020.
- Temnerud, J. and Bishop, K.: Spatial Variation of Streamwater Chemistry in Two Swedish Boreal Catchments: Implications for Environmental Assessment, <https://doi.org/10.1021/ES040045Q>, 2005.
- 710 Temnerud, J., Fölster, J., Buffam, I., Laudon, H., Erlandsson, M., and Bishop, K.: Can the distribution of headwater stream chemistry be predicted from downstream observations?, *24*, 2269–2276, <https://doi.org/10.1002/hyp.7615>, 2010.
- Terry, N., Grunewald, E., Briggs, M., Gooseff, M., Huryn, A. D., Kass, M. A., Tape, K. D., Hendrickson, P., and Lane, J. W.: Seasonal Subsurface Thaw Dynamics of an Aufeis Feature Inferred From Geophysical Methods, *125*, e2019JF005345, <https://doi.org/10.1029/2019JF005345>, 2020.
- 715 Thrush, S. F., Schneider, D. C., Legendre, P., Whitlatch, R. B., Dayton, P. K., Hewitt, hJ. E., Hines, A. H., Cummings, V. J., Lawrie, S. M., Grant, J. P., Pridmore, iR. D., Turner, S. J., and McArdle, B. H.: Scaling-up from experiments to complex ecological systems : Where to next ?, 1997.
- Toohey, R. C., Herman-Mercer, N. M., Schuster, P. F., Mutter, E. A., and Koch, J. C.: Multidecadal increases in the Yukon River Basin of chemical fluxes as indicators of changing flowpaths, groundwater, and permafrost, *43*, 12,120-12,130, <https://doi.org/10.1002/2016GL070817>, 2016.
- 720 Turetsky, M. R., Abbott, B. W., Jones, M. C., Anthony, K. W., Olefeldt, D., Schuur, E. A. G., Grosse, G., Kuhry, P., Hugelius, G., Koven, C., Lawrence, D. M., Gibson, C., Sannel, A. B. K., and McGuire, A. D.: Carbon release through abrupt permafrost thaw, *13*, 138–143, <https://doi.org/10.1038/s41561-019-0526-0>, 2020.
- 725 Vonk, J. E., Tank, S. E., Bowden, W. B., Laurion, I., Vincent, W. F., Alekseychik, P., Amyot, M., Billet, M. F., Canário, J., Cory, R. M., Deshpande, B. N., Helbig, M., Jammet, M., Karlsson, J., Larouche, J., MacMillan, G., Rautio, M., Walter Anthony, K. M., and Wickland, K. P.: Reviews and syntheses: Effects of permafrost thaw on Arctic aquatic ecosystems, *Biogeosciences*, *12*, 7129–7167, <https://doi.org/10.5194/bg-12-7129-2015>, 2015.

- Vonk, J. E., Tank, S. E., and Walvoord, M. A.: Integrating hydrology and biogeochemistry across frozen landscapes, *Nat Commun*, 10, 1–4, <https://doi.org/10.1038/s41467-019-13361-5>, 2019.
- 730 Ward, A. S., Zarnetske, J. P., Baranov, V., Blaes, P. J., Brekenfeld, N., Chu, R., Derelle, R., Drummond, J., Fleckenstein, J. H., Garayburu-Caruso, V., Graham, E., Hannah, D., Harman, C. J., Herzog, S., Hixson, J., Knapp, J. L. A., Krause, S., Kurz, M. J., Lewandowski, J., Li, A., Martí, E., Miller, M., Milner, A. M., Neil, K., Orsini, L., Packman, A. I., Plont, S., Renteria, L., Roche, K., Royer, T., Schmadel, N. M., Segura, C., Stegen, J., Toyoda, J., Wells, J., Wisnoski, N. I., and Wondzell, S. M.: Co-located contemporaneous mapping of morphological, hydrological, chemical, and biological conditions in a 5th-order mountain stream network, Oregon, USA, 11, 1567–1581, <https://doi.org/10.5194/essd-11-1567-2019>, 2019.
- 735 Weishaar, J. L., Aiken, G. R., Bergamaschi, B. A., Fram, M. S., Fujii, R., and Mopper, K.: Evaluation of Specific Ultraviolet Absorbance as an Indicator of the Chemical Composition and Reactivity of Dissolved Organic Carbon, *Environ. Sci. Technol.*, 37, 4702–4708, <https://doi.org/10.1021/es030360x>, 2003.
- Wiens, J. A.: Spatial Scaling in Ecology, 3, 385–385, <https://doi.org/10.2307/2389612>, 1989.
- 740 Wolock, D. M., Fan, J., and Lawrence, G. B.: Effects of basin size on low-flow stream chemistry and subsurface contact time in the Neversink River watershed, New York, 11, 1273–1286, [https://doi.org/10.1002/\(SICI\)1099-1085\(199707\)11:9<1273::AID-HYP557>3.0.CO;2-S](https://doi.org/10.1002/(SICI)1099-1085(199707)11:9<1273::AID-HYP557>3.0.CO;2-S), 1997.
- Wrona, F. J., Johansson, M., Culp, J. M., Jenkins, A., Mård, J., Myers-Smith, I. H., Prowse, T. D., Vincent, W. F., and Wookey, P. A.: Transitions in Arctic ecosystems: Ecological implications of a changing hydrological regime, 121, 650–674, <https://doi.org/10.1002/2015JG003133>, 2016.
- 745 Yi, Y., Gibson, J. J., Hélie, J.-F., and Dick, T. A.: Synoptic and time-series stable isotope surveys of the Mackenzie River from Great Slave Lake to the Arctic Ocean, 2003 to 2006, *Journal of Hydrology*, 383, 223–232, <https://doi.org/10.1016/j.jhydrol.2009.12.038>, 2010.
- Yoshikawa, K., Hinzman, L. D., and Kane, D. L.: Spring and aufeis (icing) hydrology in Brooks Range, Alaska, 112, G04S43, <https://doi.org/10.1029/2006JG000294>, 2007.
- 750 Zarnetske, J. P., Bouda, M., Abbott, B. W., Saiers, J., and Raymond, P. A.: Generality of Hydrologic Transport Limitation of Watershed Organic Carbon Flux Across Ecoregions of the United States, 45, 11,702–11,711, <https://doi.org/10.1029/2018GL080005>, 2018.
- Zarnetske, J. P., Bowden, W. B., Abbott, B. W., and Shogren, A. J.: High-frequency dissolved organic carbon and nitrate from the Kuparuk River outlet near Toolik Field Station, Alaska, summer 2017–2019, <http://dx.doi.org/10.6073/pasta/990958760c13cdd55b574c5202dc19b7>, 2020a.
- 755 Zarnetske, J. P., Bowden, W. B., Abbott, B. W., and Shogren, A. J.: High-frequency dissolved organic carbon and nitrate from the Oksrukuyik Creek outlet near Toolik Field Station, Alaska, summer 2017–2019, <http://dx.doi.org/10.6073/pasta/5d63c098887205597ce0df929467168c>, 2020b.
- 760 Zarnetske, J. P., Bowden, W. B., Abbott, B. W., and Shogren, A. J.: High-frequency dissolved organic carbon and nitrate from the Trevor Creek outlet near Toolik Field Station, Alaska, summer 2017–2019, <http://dx.doi.org/10.6073/pasta/3bd6a1d2d9487546f32d46d2943c6e43>, 2020c.
- Zimmer, M. A., Bailey, S. W., McGuire, K. J., and Bullen, T. D.: Fine scale variations of surface water chemistry in an ephemeral to perennial drainage network, 27, 3438–3451, <https://doi.org/10.1002/hyp.9449>, 2013.

Figures & Tables



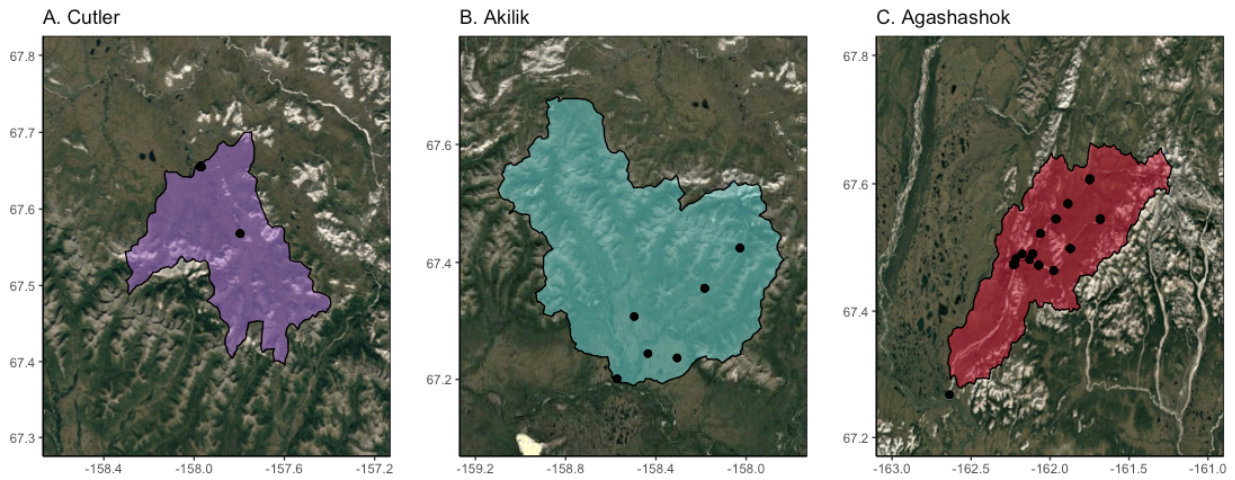
770 **Figure 1. Regions of northern Alaska associated with the Arctic Long-Term Ecological Research site at Toolik Field Station (TFS) and National Park Service (NPS) and U.S. Geological Survey (USGS) watersheds. Map created in R Studio (version 1.2.1335) with base imagery from ESRI and Google Earth (Version 7.3.3.7786).**



775

Figure 2. Synoptic sampling sites (black points) with subcatchment delineations from three watersheds related to the Arctic Long-Term Ecological Research site at Toolik Field Station (TFS) on the North Slope of Alaska. Study watersheds include the A. Kuparuk River (blue), B. Oksrukuyik Creek (orange), and C. Trevor Creek (green). Scale bars in km. The Arctic LTER monitoring stations are denoted by red points and described further in Shogren et al. 2021. Map created in R Studio (version 1.2.1335) with base imagery from ESRI and Google Earth (Version 7.3.3.7786).

780



785 **Figure 3. Synoptic sampling sites in three NPS/USGS watersheds. Study watersheds include the A. Cutler, B. Akilik, and C. Agashashok Rivers. Map created in R Studio (version 1.2.1335) with base imagery from ESRI and Google Earth (Version 7.3.3.7786).**

790

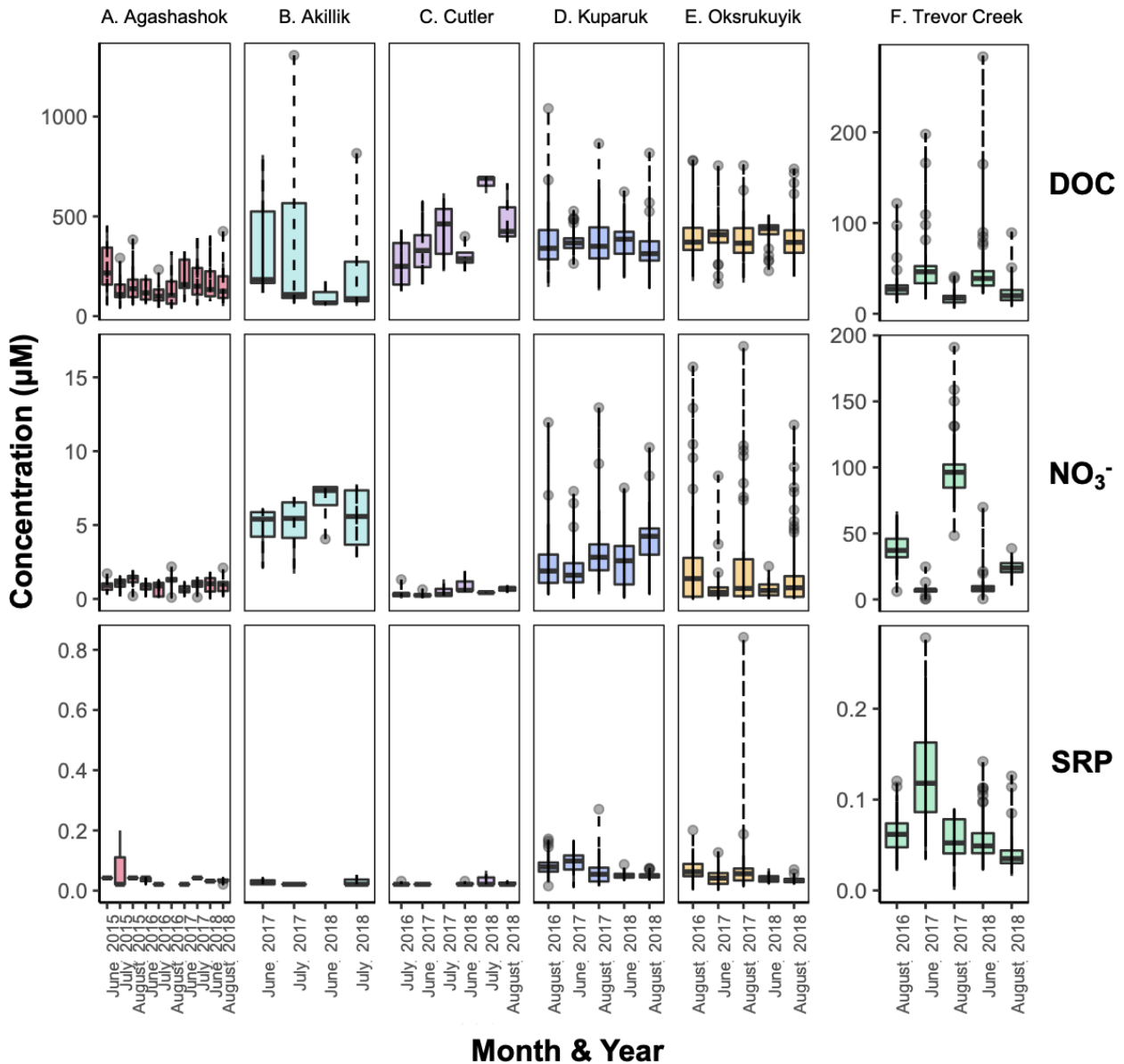
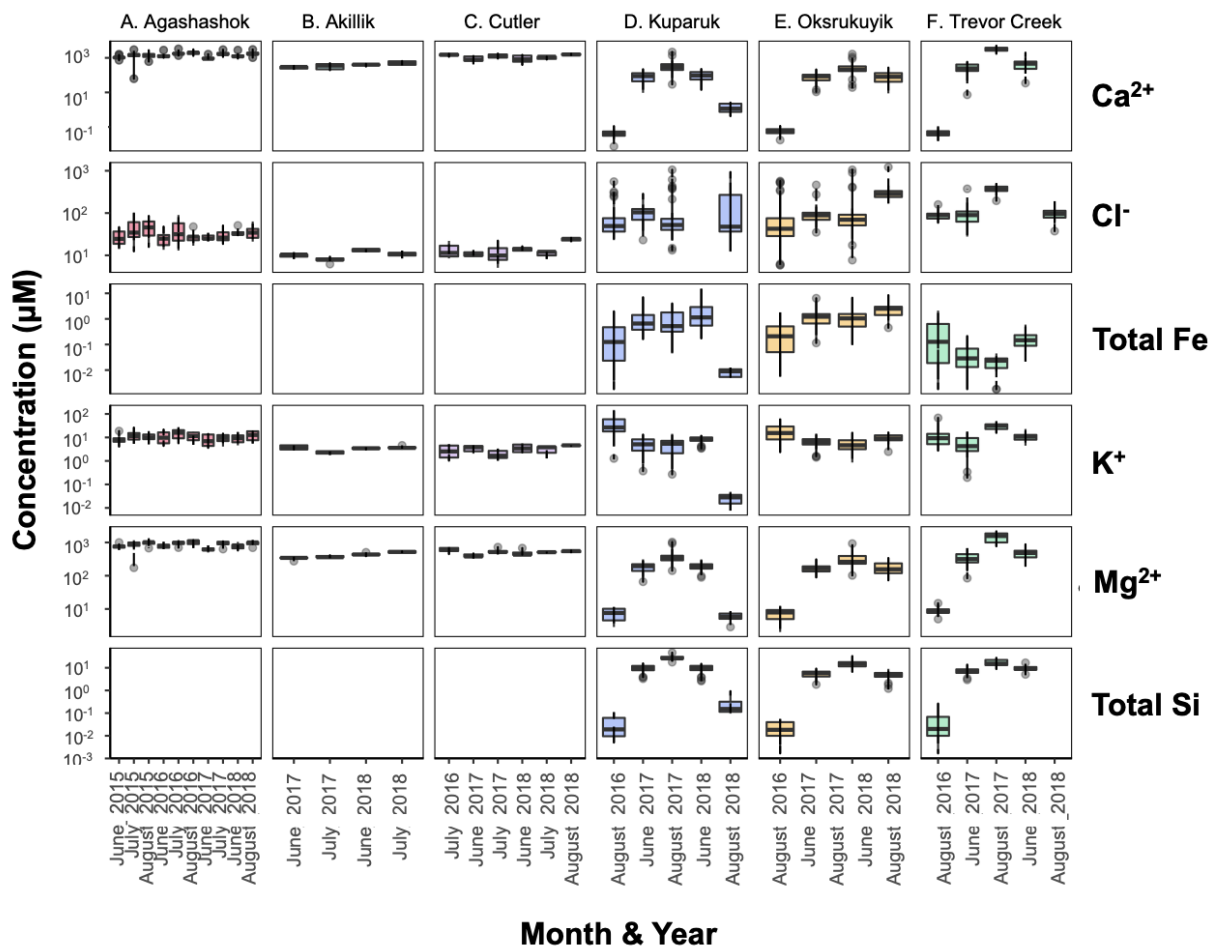
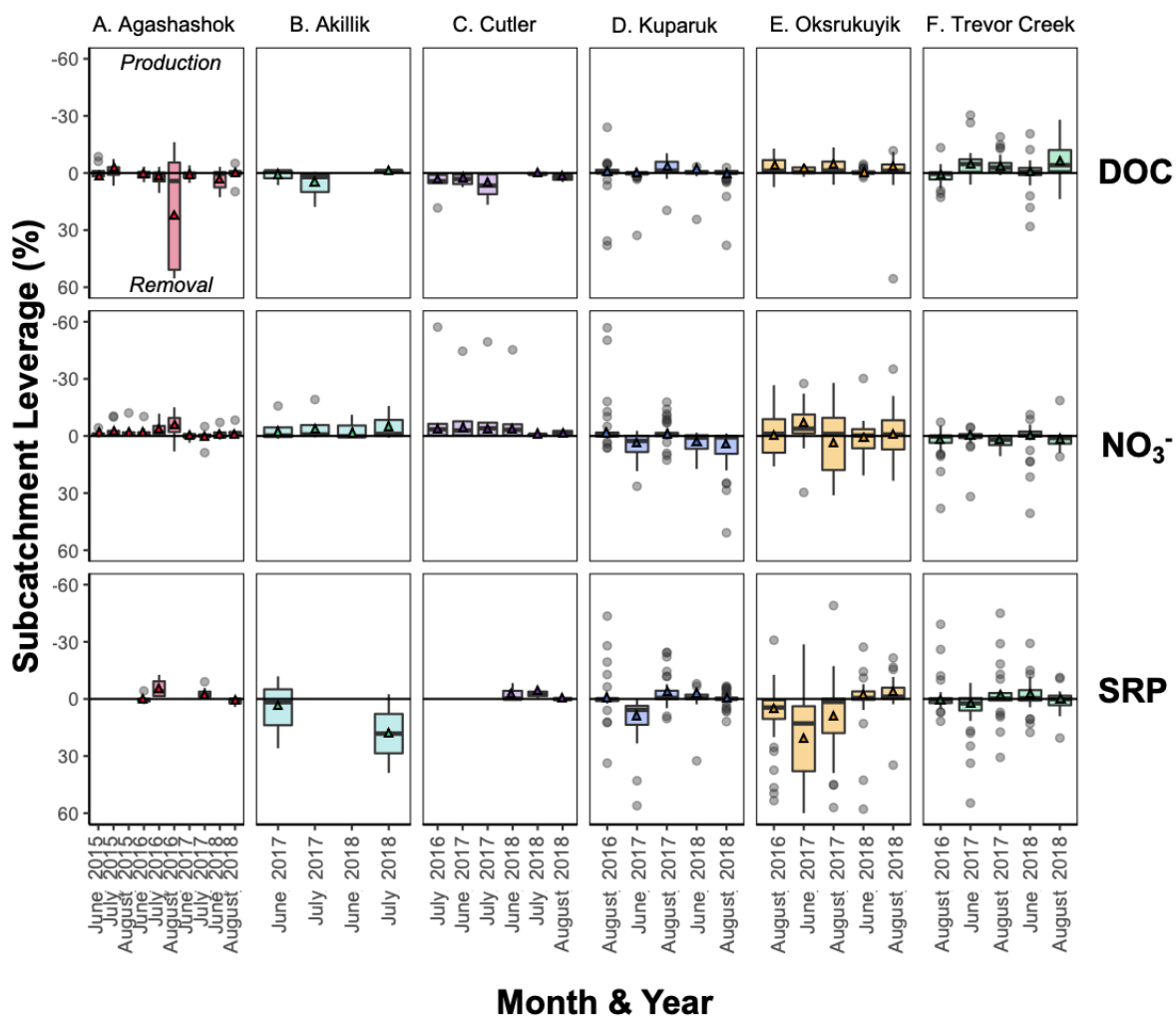


Figure 4: Boxplots of dissolved organic carbon (DOC, top row), nitrate (NO_3^- , middle row), and soluble reactive phosphorus (SRP, bottom row) concentration ranges (in μM) in the (A) Agashashok River, (B) Akilik River, (C) Cutler River, (D) Kuparuk, (E) Oksrukuyik Creek, and (F) Trevor Creek watersheds across all years and seasons sampled. Each box encapsulates values within the lower 25th and upper 75th quartiles respectively, while the whiskers represent the minimum and maximum quartiles. Within each box, the horizontal line represents the median leverage value. Data points outside the whiskers represent values above/below 1.5x the IQR threshold.

795

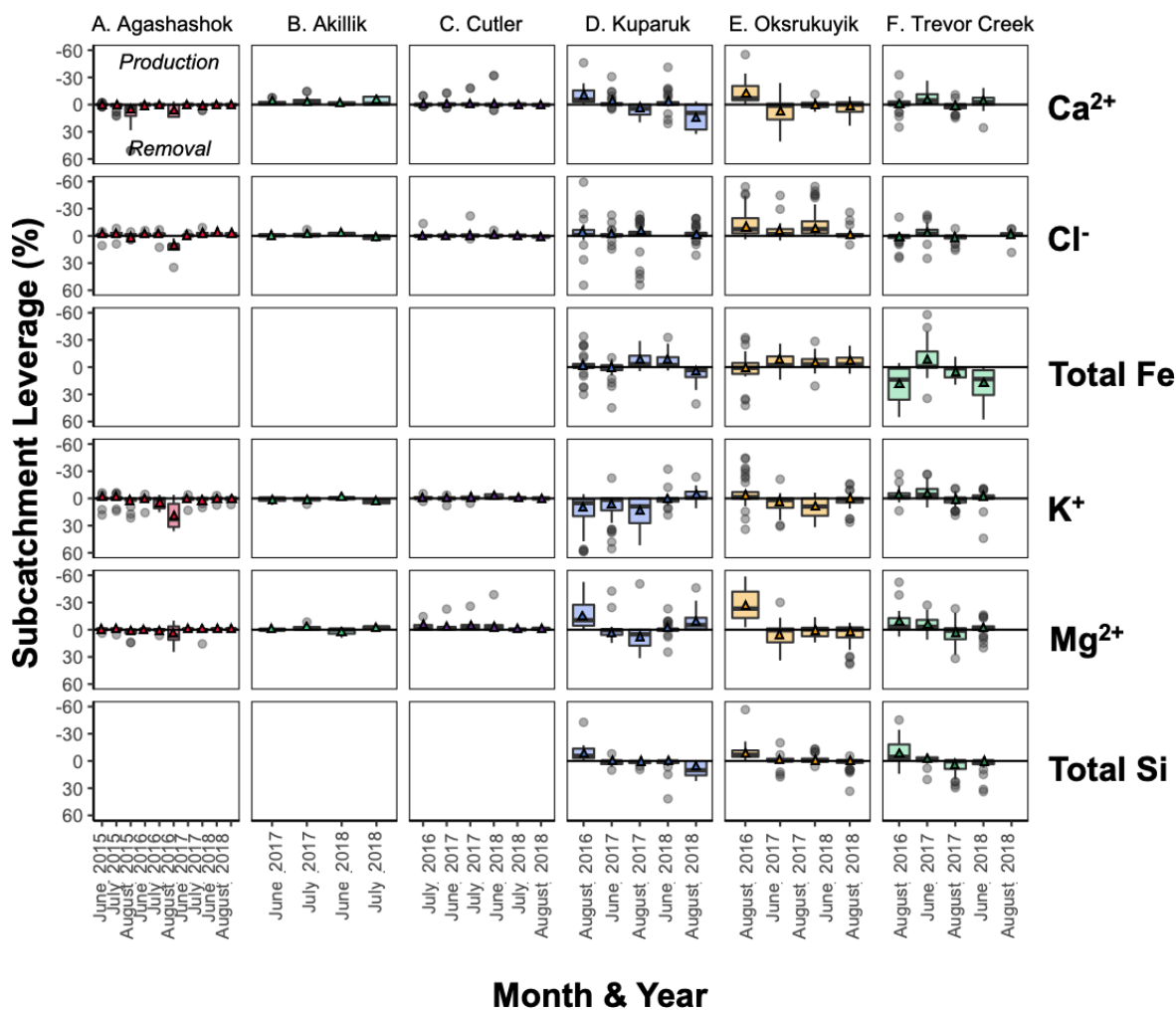


805 **Figure 5: Boxplots of Ca²⁺, Cl⁻, Fe (NPS/USGS = Total; TFS = nominally dissolved), K⁺, Mg²⁺, and**
Total Si concentration ranges (in μM) in the (A) Agashashok River, (B) Akilik River, (C) Cutler
River, (D) Kugaruk River, (E) Oksrukuyik Creek, and (F) Trevor Creek watersheds across all
years and seasons sampled. Each box encapsulates values within the lower 25th and upper 75th
810 **quartiles respectively, while the whiskers represent the minimum and maximum quartiles. Within**
each box, the horizontal line represents the median leverage value. Data points outside the
whiskers represent values above/below 1.5x the IQR threshold.

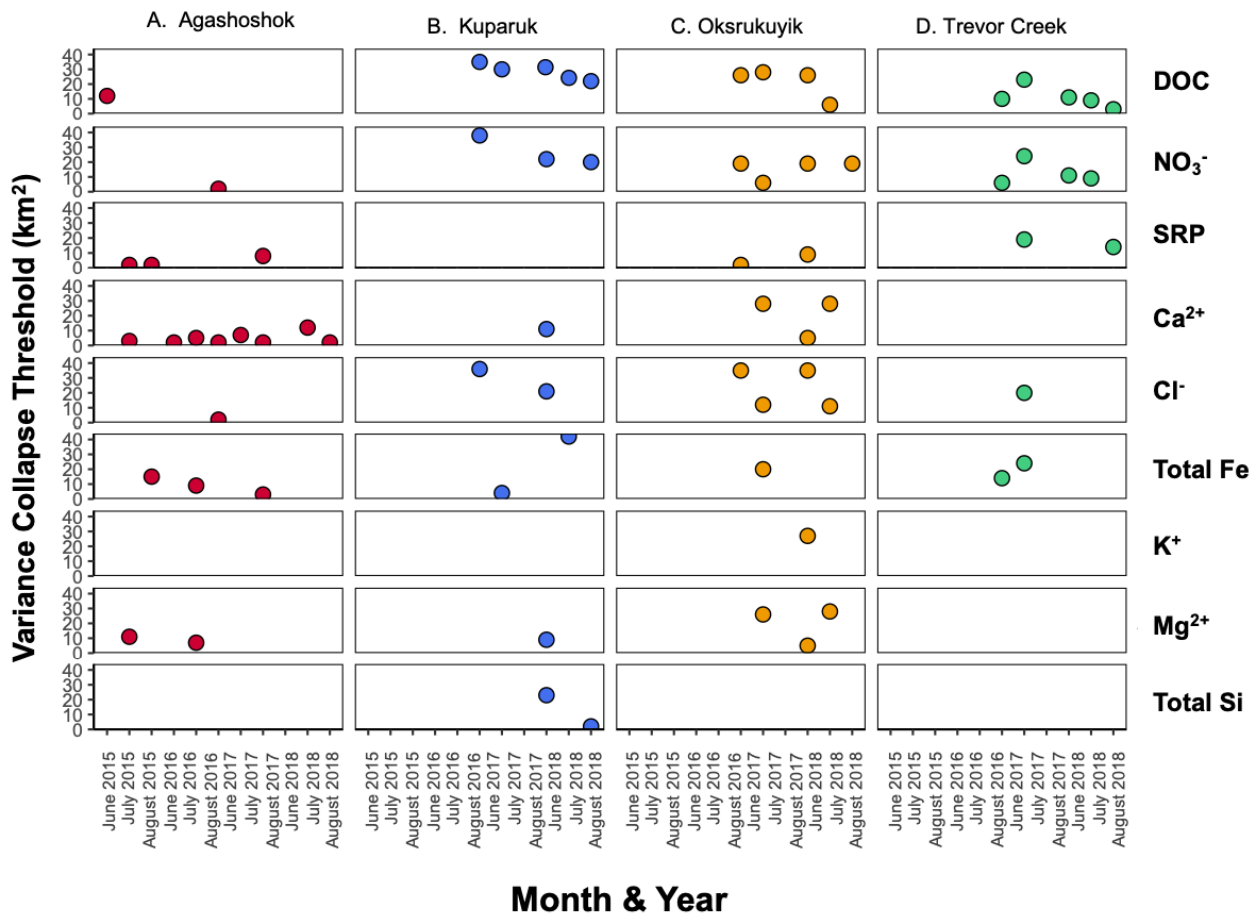


815 **Figure 6: Boxplot of subcatchment leverage for select reactive solutes (DOC, NO₃⁻, and SRP) in the (A) Agashashok River, (B) Akilik River, (C) Cutler River, (D) Kugaruk River, (E) Oksrukuyik Creek, and (F) Trevor Creek watersheds across all years and seasons sampled. Note reversed axes for ease of interpretation: negative values above the 0 line indicate production, positive values below the 0 line indicate removal. Each box encapsulates values within the lower 25th and upper 75th quartiles respectively, while the whiskers represent the minimum and maximum quartiles. Within each box, the horizontal line represents the median leverage value and the colored triangle lies at the mean. Data points outside the whiskers represent values above/below 1.5x the IQR threshold.**

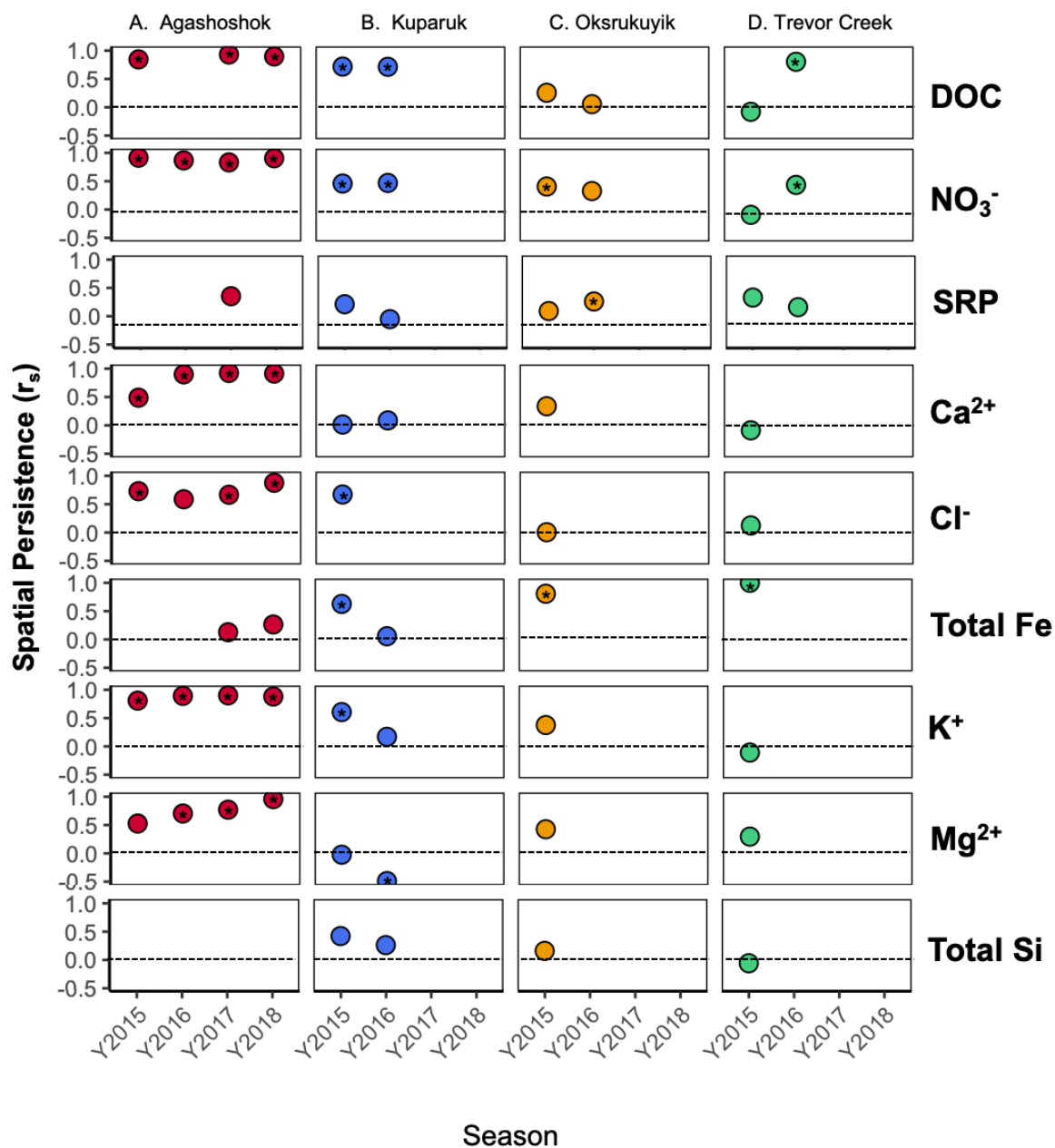
820



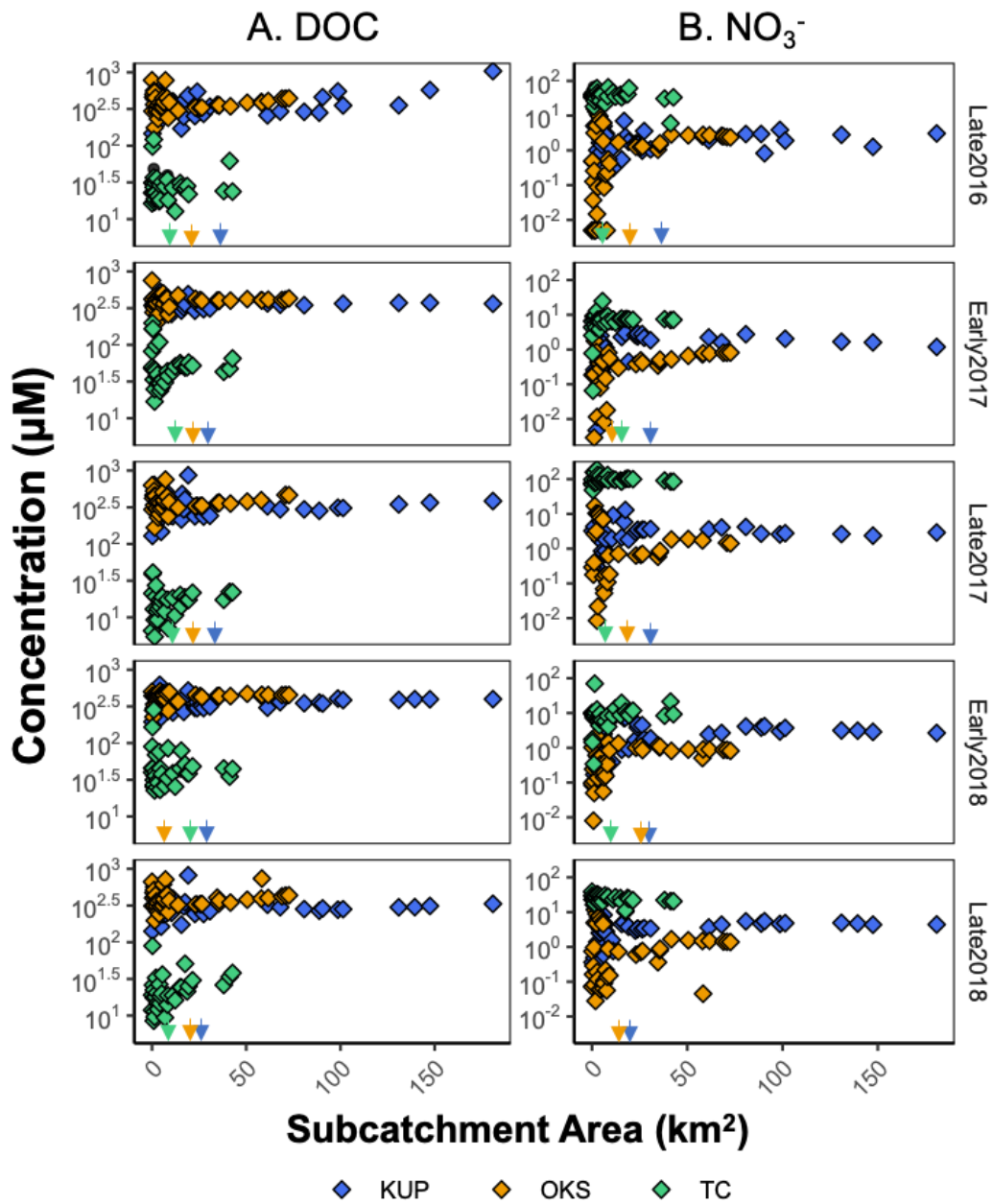
825 **Figure 7: Boxplot of subcatchment leverage for select conservative solutes (Ca²⁺, Cl⁻, Fe**
(NPS/USGS = Total; TFS = nominally dissolved), K⁺, Mg²⁺, and Total Si) in the (A) Agashashok
River, (B) Akilik River, (C) Cutler River, (D) Kugaruk River, (E) Oksrukuyik Creek, and (F)
Trevor Creek watersheds across all years and seasons sampled. Note reversed axes for ease of
interpretation: negative values above the 0 line indicate production, positive values below the 0
830 **line indicate removal. Each box encapsulates values within the lower 25th and upper 75th quartiles**
respectively, while the whiskers represent the minimum and maximum quartiles. Within each
box, the horizontal line represents the median leverage value and the colored triangle lies at the
mean. Data points outside the whiskers represent values above/below 1.5x the IQR threshold.



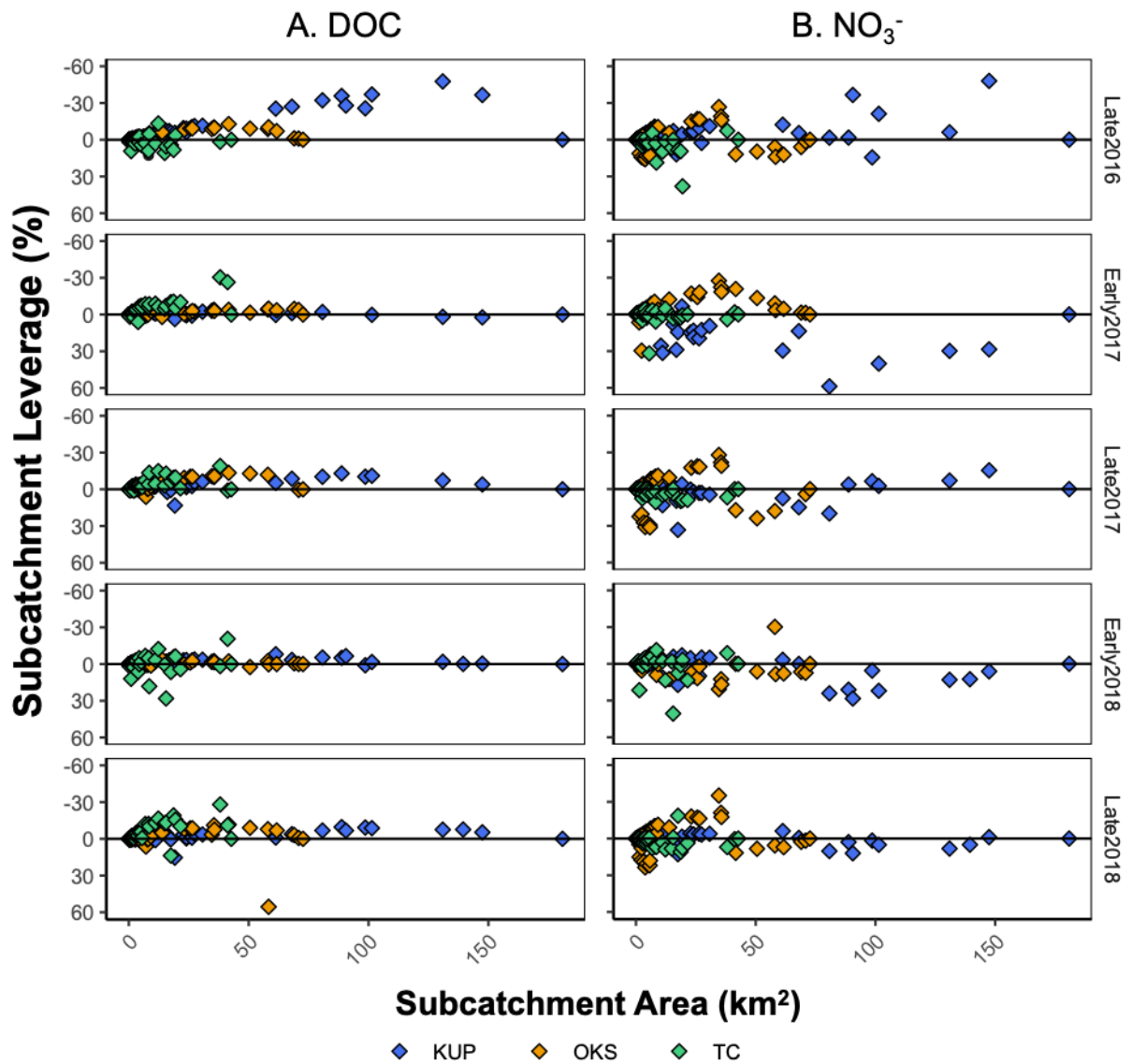
835 **Figure 8: Figure 8: Scatter plot of variance collapse threshold for each repeated sampling for the**
A. Agashashok River, B. Kugaruk River, C. Oksrukuyik Creek, and D. Trevor Creek watersheds
for select reactive (e.g., DOC, NO₃⁻, and SRP) and conservative solutes (Ca²⁺, Cl⁻, Fe (NPS/USGS
= Total; TFS = nominally dissolved), K⁺, Mg²⁺, and Total Si). When data were not present, there
was no significant collapse detected. Variance collapse thresholds are not shown for the Akilik
840 **and Cutler Rivers, as these thresholds were often non-significant.**



845 **Figure 9: Scatter plot of spatial stability (r_s) for each repeated sampling for the A. Kuparuk River, B. Oksrukuyik Creek, and C. Trevor Creek watersheds for select reactive (e.g., DOC, NO₃⁻, and SRP) and conservative solutes (Ca²⁺, Cl⁻, Fe (NPS/USGS = Total; TFS = nominally dissolved), K⁺, Mg²⁺, and Total Si). When data were not present, there is no spatial stability reported. When Spearman's Rank Correlation (r_s) is significant, this is denoted by an asterisk (*) within the point.**



850 **Figure 10: Scatter plot of log-scale A. DOC and B. NO₃⁻ concentrations (µM) across subcatchment area (km²) or each repeated sampling in the Kuparuk River (blue points), Oksrukuyik Creek (orange points), and Trevor Creek (green points) watersheds. Significant variance collapse thresholds are represented by a colored arrow.**



855

Figure 11: Scatter plot of A. DOC and B. NO₃⁻ leverages across subcatchment area (km²) or each repeated sampling in the Kuparuk River (blue points), Oksrukuyik Creek (orange points), and Trevor Creek (green points) watersheds. Note reversed axes for ease of interpretation: negative values above the 0 line indicate production, positive values below the 0 line indicate removal.

860

Tables

865 **Table 1. Summary of site characteristics for the watersheds where synoptic samplings were conducted. The descriptions are considered representative of the major landform types within the TFS and NPS/USGS watersheds.**

	Site	Slope (°)	Mean Elevation (m)	Geologic Setting	Permafrost Zone	Primary vegetation	Number of sampling sites	Total Drainage Area (km ²)
TFS	Kuparuk River	Low (3.1)	988	Sagavanirktok Old Glaciated Uplands	Continuous permafrost	Wet acidic tundra	45	92.5
	Oksrukuyik Creek	Low (3.2)	862	Sagavanirktok Young Glaciated Valleys	Continuous permafrost	Wet acidic tundra	42	72.6
	Trevor Creek	High (9.4)	1595	Sagavanirktok Young Glaciated Valleys	Continuous permafrost	Alpine valley	35	42.7
NPS/ USGS	Agashashok River	High (9.3)	317	Sedimentary carbonate and non-carbonate lithology	Continuous permafrost	Boreal spruce forest, arctic tundra	9	1058.0
	Cutler River	High (8.0)	644	Quaternary, noncarbonate deposits (glaciolacustrine)	Continuous permafrost	Boreal spruce forest, arctic tundra	6	566.7
	Akillik River	High (14.8)	447	Quaternary, silt and peat	Discontinuous permafrost	Boreal spruce forest, arctic tundra	5	262.1

870 **Table 2: Description of the sampling campaign regimes, including dates for each campaign, for the TFS and NPS/USGS watersheds.**

	Site	Years of repeated synoptic sampling	Number of sampling events	Sampling Dates	Seasonal Sampling
TFS	Kuparuk River	2016-2018	5	2016: 8/26 2017: 6/5; 8/27 2018: 6/6; 8/24	June, August
	Oksrukuyik Creek	2016-2018	5	2016: 8/17 2017: 6/3; 8/24 2018: 6/4; 8/23	June, August
	Trevor Creek	2016-2018	5	2016: 8/22 2017: 6/7; 8/31 2018: 6/8; 8/28	June, August
NPS/ USGS	Agashashok River	2015-2019	10	2015: 6/9-6/12; 8/7-8/11; 9/16-9/19 2016: 6/7-6/12; 8/9-8/12; 9/8-9/9 2017: 6/6-6/8; 8/16-8/18 2018: 6/11-6/12; 9/2-9/6	June, August, Sept
	Cutler River	2015-2019	5	2016: 8/14-8/15 2017: 6/10; 8/20-8/21 2018: 6/14; 8/31-9/1	June, August, Sept
	Akillik River	2015-2019	4	2017: 6/11-6/12; 8/22-8/23 2018: 6/13; 8/30	June, August, Sept

875 **Table 3. Summary of sample processing and analytical methods used for the dataset for A. TFS and B. NPS/USGS field sites. Expanded table in supplement.**

A. TFS					
	Parameter	Units	Instrument	Analytical Method	Detection Limit
Watershed Characteristics	Drainage Area	km ²			
	Slope (mean)	Degrees			
	Slope (standard deviation)	Degrees	Arc-GIS	Spatial analysis	
	Roughness (mean)	NDVI			
	Roughness (standard deviation)	NDVI			
Water Quality Measurements	Temperature	°C			
	Specific Conductivity	µS/cm	YSI Pro Plus Multiparameter Mete	Analyzed in the field with a handheld field probe	
	pH	pH			
	O ₂	% Sat	YSI ProODO Dissolved Oxygen Meter		
Water Chemistry (post-filtering)	Turbidity	NTU	Forest Technology Systems (FTS) DTS-12 digital turbidity sensor		Nephelometric geometry
	DOC	µM		Combustion catalytic oxidation method	0.3 µM
	TDN	µM	Shimadzu TOC-LCPH with TN	High-Temperature Catalytic Combustion and Chemiluminescence Detectio	0.28µM
	N-NO ₃	µM		Cadmium Reduction	0.03µM
	N-NH ₄	µM	Lachat Quikchem Flow Injection Analysis System	Sodium salicylate-based procedure that requires a standard heating unit and is read at 660 nm	0.3µM
	SRP	µM	Shimadzu UV-2600 spectrophotomete r	Colorimetric analysis using an ammonium molybdate-based reagent. (Although technically USGS refers to this as the Ascorbic Acid method...)	0.05µM

PP	μM			Same as above, preceded by combustion at 500C and a hydrochloric acid digestion	0.05μM
TDP	μM			Same as SRP, preceded by a potassium persulfate digestion.	0.05μM
F, Acetate, Formate, Cl, NO ₂ , Br, SO ₄ , PO ₄ , Li, Na, NH ₄ , K, Mg, Ca	μM	Thermoscientific Dionex ICS-2100 Integrated IC System with Electrolytic Eluent Generation with an AS-AP Autosampler		Ion Chromatography	0.05 μM
nPOC	mg/L				0.3 μM
Spectral Slope Ratio	Unitless	Shimadzu TOC-LCPH with TN		Combustion catalytic oxidation method	
SUVA ₂₅₄	L mgC ⁻¹ m ⁻¹				
Al, As, B, Ba, C, Cd, Co, Cr, Cu, Fe, K, Mg, Mn, Mo, Na, Ni, P, Pb, S, Se, Si, Sr, Ti, V, Zn	μM	ICP-MS		Inductively Couple Plasma Mass Spectrometry (ICP)	0.02 mg/L
Alkalinity	meq/L	Accumet AB200 pH meter		Samples individually titrated with 0.18N sulfuric acid	0.2 meq/L

B. NPS

	Parameter	Units	Instrument	Specific Method	Detection Limit
Watershed Characteristics	Drainage Area	km ²	Arc-GIS	Watershed delineation	
	Slope (mean)	Degrees			
	Slope (standard deviation)	Degrees			
	Roughness (mean)	NDVI			
	Roughness (standard deviation)	NDVI			

Water Quality Measurements (Taken in the field)	Temperature	°C	YSI Pro Plus Multiparameter Meter			
	Specific Conductivity	µS/cm				
	pH	pH				
	O ₂	% Sat	YSI ProODO Dissolved Oxygen Meter			
Water Chemistry (post-filtering)	DOC	mg/L	O.I Analytical Model 700 TOC Analyzer	Platinum-catalyzed persulfate wet oxidation method	4 ug/L	
	TDN	mg/L	Technicon Auto-Analyzer II	Persulfate digest	0.01 mg/L	
	NO ₃ +NO ₂	mg/L		Cadmium reduction	0.001 mg/L	
	NH ₄	mg/L	Labchat QuikChem 8500	Colorimetric	0.01 mg/L	
	SRP	mg/L		Ascorbic acid method	0.001 mg/L	
	TDP	mg/L	Technicon Auto-Analyzer II	Persulfate digest	0.002 mg/L	
	Cl, SO ₄	mg/L	Dionex 1500 IC	Ion Chromatography	0.01 mg/L	
	Na, K, Mg, Ca, Fe	mg/L	Shimadzu AA-7000	Flame atomic absorption spectroscopy	0.01, 0.03, 0.02, 0.06, 0.06 mg/L	
	SUVA ₂₅₄	L mgC ⁻¹ m ⁻¹		Spectrophotometer		
	Alkalinity	mgCaCO ₃ /L	ManTech PC-Titrate Auto Titrator System	Titration to 4.5, use 0.02N Na ₂ CO ₃ and 0.02 N H ₂ SO ₄	0.2 mg CaCO ₃ /L	
	DIC	mg/L	Shimadzu TOC-VCSH Combustion Analyzer	Combustion catalytic oxidation method	0.05 mg/L	